FACULTAT
DE CIÈNCIES
I TECNOLOGIA
UVIC | UVIC·UCC

quantitative
bio
imaging

Final Degree Project

INITIAL EXPLORATION OF VASCULAR ENDOTHELIAL GROWTH FACTOR EFFECT ON FIBROBLASTS IN THE CONTEXT OF WOUND HEALING

FRANCISCO NAVARRO PÁEZ

Biotechnology Degree

Tutor: Marta Cullell-Dalmau

Vic, June of 20

Acknowledgments

First of all, I would like to thank my tutor Marta Cullell for the support she has given me throughout the development of this final degree project, I appreciate all the knowledge she has shared with me and for taking such good care of me as much as she has done.

I would also like to acknowledge Dr. Carlo Manzo for all the help he has provided in the field of image and statistical analysis of the data, a key area for the realization of this final degree project.

I am grateful for all the advice and help Montse Masolivar, Mº Cristina Martín and Dr. Marta Otero have provided me in the laboratory and their predisposition to help me in anything without hesitating.

I feel very fortunate and honoured to have been able to perform my final degree project in the Quantitative Bioimaging Laboratory of the University of Vic. I will, for sure, cherish all the memories I have made here in this final year of the degree.

Abstract

Title: Initial Exploration of Vascular Endothelial Growth Factor Effect on Fibroblast in the Context of Wound Healing
Author: Francisco Navarro Páez
Supervisor: Marta Cullell-Dalmau
Date: June 2020
Key words: dermalfibroblasts; integrin $\alpha_5\beta_1$; vascular endothelial growth factor A; vascular endothelial growth factor receptor 1; solid-barrier wound healing assay; cell tracking; migration; single particle tracking; diffusion.

Fibroblasts are key elements on the wound healing process, to close the wound they must migrate, migration is mediated by transmembrane proteins called integrins, especially by integrin $\alpha_5\beta_1$. Anomalous integrin function may lead to a compromised wound healing rate, a determinant factor for proper integrin function is their ability to interact with growth factors that coordinate the wound healing process. One of the most important growth factors in the context of wound healing is Vascular Endothelial Growth Factor A (VEGF-A), the vast majority of studies related to VEGF-A have their focal point on endothelial cells due to VEGF-A's angiogenic stimulation qualities. However, fibroblasts express its receptor (VEGF-R1) and thus, should be able to respond to its stimulus. For these reasons, we have decided to study the effect on VEGF-A on fibroblasts.

First, we carried out a protein-protein interaction database search to find out any interactions between $\alpha_5\beta_1$, VEGF-A and VEGF-R1. This was then complemented by performing experiments at a cellular level by designing a solid-barrier wound healing assay to assess fibroblast collective migration and by implementing a cell tracking pipeline to assess fibroblast individual migration and at a molecular level by performing single particle tracking experiments to study integrin $\alpha_5\beta_1$ diffusion on fibroblasts under VEGF-A treatment.

Due to the protein-protein interaction database search, we found out that there are many indirect interactions between our proteins of interest and only one direct interaction ($\alpha_5\beta_1$ and the soluble version of VEGF-R1) but these interactions (direct and indirect) have only been assessed on endothelial cells, not fibroblasts. We have set up a cell tracking protocol and as a result, we have seen a significant reduction in cell migration under VEGF-A treatment. Moreover, the single particle tracking experiments show a reduction in the percentage of immobile integrins $\alpha_5\beta_1$ and an increase in mobile integrin velocity under VEGF-A treatment.

Unfortunately, due to the COVID-19 lockdown, we could not make replicates of the experiments so once the laboratories re-open, they must be done again to be able to contrast the results we have obtained.

Resum

Títol: Exploració inicial del efecte del factor de creixement vascular endotelial en els fibroblasts en el context de la cicatrització
Autor: Francisco Navarro Páez
Supervisor: Marta Cullell-Dalmau
Data: Juny 2020
Paraules claus: dermofibroblasts; integrina α5β1; Factor de creixement endotelial vascular; receptor del factor de creixement endotelial vascular; assaig de cicatrització; seguiment cel·lular; migració; seguiment de partícules individuals; difusió.

Els fibroblasts són cèl·lules clau en el procés de cicatrització, concretament per a tancar la ferida han de migrar, i la migració esta mediada per proteïnes transmembrana anomenades integrines, especialment per la integrines $\alpha_5\beta_1$. Una funció anòmala de les integrines pot comprometre el temps de cicatrització. Un dels factors que modulen la correcta activitat d'aquestes integrines és la seva capacitat per a interaccionar amb factors de creixement, els quals coordinen el procés de cicatrització. Un dels factors de creixement mes importants en el context de la cicatrització és el Factor de Creixement Endotelial Vascular A (VEGF-A) però la majoria dels estudis sobre aquest factor de creixement estan centrats en el seu efecte en les cèl·lules endotelials a causa de la seva capacitat pro-antogènica. No obstant això, els fibroblasts expressen el seu receptor (VEGF-R1) i per tant haurien de ser capaços de respondre davant el seu estímul. Per aquestes raons es va decidir estudiar l'efecte que té el VEGF-A en els fibroblasts.

Primer es va realitzar una cerca a base de dades d'interaccions proteiques per a trobar possibles interaccions entre la integrina $\alpha_5\beta_1$, el VEGF-A i el VEGF-R1. Després aquesta cerca es va complementar amb experiments a dos nivells. Primer a nivell cel·lular, dissenyant un assaig de cicatrització que no danyés la matriu extracel·lular i implementant un mètode de seguiment cel·lular, i a un nivell molecular mitjançant estudis de seguiment de partícula individual per a avaluar el canvi de difusió de la integrina $\alpha_5\beta_1$ en fibroblasts tractats amb VEGF-A.

Gràcies a la cerca a bases de interaccions proteiques, descobrim que les nostres proteïnes d'interès interactuen entre si de manera indirecta gràcies a altres proteïnes i només es coneix a dia d'avui una interacció directa i és entre la versió soluble del VEGF-R1 i la integrina $\alpha_5\beta_1$. No obstant això, totes aquestes interaccions només s'han descrit en cèl·lules endotelials i no en fibroblasts. Hem posta a punt un protocol per el seguiment de cèl·lules individuals i gràcies a això em trobat diferències significatives en la migració cel·lular i una reducció de la proporció de integrines $\alpha_5\beta_1$ immòbils i en les velocitats de les mòbils quan son tractats amb VEGF-A.

Malauradament, per culpa del COVID-19 no em pogut fer repliques dels experiments y s'haurien de contrastar quan es reobrin el laboratoris.

Index

Glossary

ECM: Extracellular matrix.

FN: Fibronectin.

PRP: platelet-rich plasma.

GF: growth factor.

GFR: growth factor receptor.

VEGF-A: Vascular endothelial growth factor A.

VEGF-R1: vascular endothelial growth factor receptor 1.

SPT: Single particle tracking.

Ab: Antibody.

hAb: Reduced antibody.

TIRF: Total internal reflection fluorescence.

QD: Quantum dots.

MSD: Mean squared displacement.

PDSD: Analysis of the probability distribution of square displacements

FBS: Fetal bovine serum

BSA: Bovine serum albumin

PDMS: Polydimethylsiloxane

PDL: Population doubling levels.

Table List

Figure List

1. Introduction

The number of people suffering from chronic wounds or wound healing problems is on the increase and has boosted due to the ageing population. 1-2% of the developed country's population will suffer a wound that will not cure and become chronic during their lifetime. This not only has a negative impact on people's lives but also takes a toll on the health budget (2-3% of the total budget) in said developed countries [1]. Hence, there is a demand for a better comprehension of their causes as well as the mechanism underlying the involved cellular processes. This will be indispensable to improve and design more effective therapies.

Anomalous integrin function and/or abnormal integrin expression is known to contribute to impaired wound healing. One factor influencing integrin-mediated migration and signalling is their ability to interact with growth factor and their receptors. With the popularity of growth factors as a treatment for wounds over the past years, specially platelet rich plasma (PRP), it is crucial to assess their effects on integrins. To date, the majority of studies examining VEGF (major growth factor in PRP) in wound healing have focused on VEGF as an angiogenesis-mediator. As a result, any findings have been attributed to endothelial cells' response to VEGF. The effect on non-endothelial cells such as fibroblasts, which play a decisive role in wound healing, is yet to be explored in depth [2].

This final degree project has been carried out in the Quantitative Bio-Imaging Laboratory (QuBI Lab) of the University of Vic (UVic-UCC). This research group, directed by Dr. Carlo Manzo, focuses its interests on the study of molecular mechanisms in cellular biophysics, with a focal point on the spatio-temporal organization and dynamics of cell membrane components in health and disease. In particular, the final degree project is part of Marta Cullell's doctorate/ research line which deals with the study of integrin α5β1 role in human skin wound healing. This topic converges with another UVic research group, the Tissue Repair and Regeneration (TR2 Lab) whose aim is to characterize the molecular composition of PRP and variability between patients as a treatment for chronic wounds.

1.1 Human Skin

The skin is the largest organ of the human body and defines the boundary between the body and its surroundings, thus allowing vital bodily functions to occur within a controlled physiological environment [3]. It has several functions such as thermoregulation, blood reservoir, protection, cutaneous sensation and synthesis of vitamin D. Human skin is a stratified epithelium, meaning it is organised by layers [4], these layers are the epidermis and the dermis. (See Figure 1).

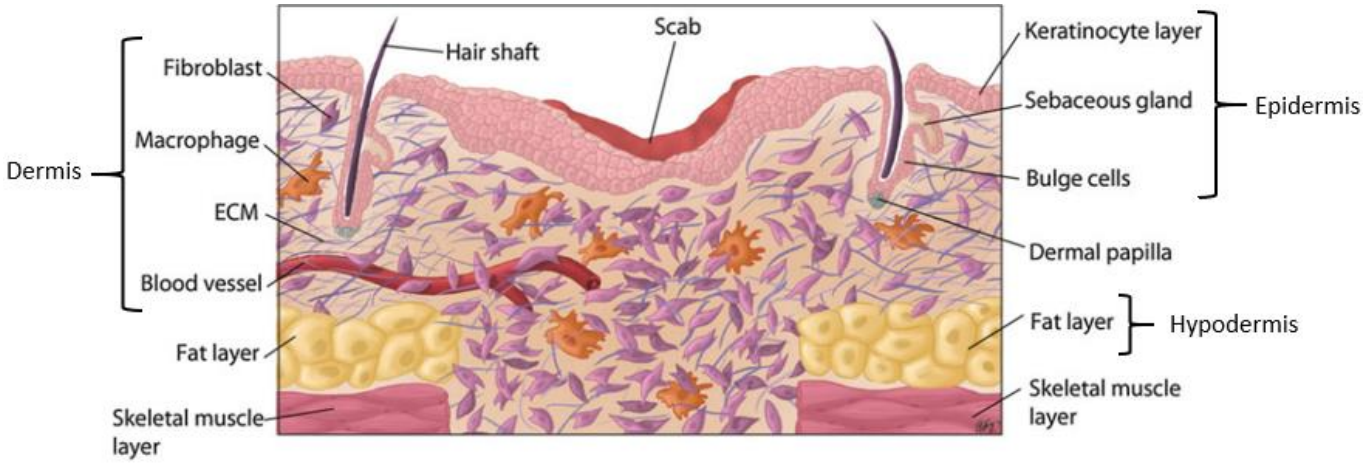

Figure 1: Human Skin Diagram. The different layers (Epidermis, Dermis and Hypodermis) are represented along with other skin components such as ECM, blood vessels, Fibroblasts and Keratinocytes. Figure adapted from:[5].

The epidermis (epithelial tissue) is composed of keratinocytes, melanocytes, Langerhans cells and Merkel cells (See Figure 1). The epidermis can be further divided into layers (outermost to innermost): Stratum Corneoum, Stratum Lucidum, Stratum Spinosum and Stratum Basale [3]. Cells forming the epidermis have a large number of tight junctions that holds them together.

The dermis (connective tissue) is under the epidermis and it is composed principally of fibroblasts and extracellular matrix (ECM), macrophages and adipocytes can also be present but not as frequently (See Figure 1). One of the most important functions of the dermis is nutrient and oxygen delivery and waste removal from the avascular epidermis because the dermis is vascularised and innervated [3].

Extracellular matrix and fibroblasts will be further discussed in section 1.3 and 1.4. due to their importance.

1.2 Wound Healing Process

A wound is an injury that breaks the continuity of the tissues, in our area of study this tissue is the skin. The wound healing process involves spatial and temporal synchronization of epithelial cells, fibroblasts, immune cells and endothelial cells which follow consecutive steps to ensure a proper wound repair, this synchronization is orchestrated by cytokines and growth factors. This event can be divided into four overlapping phases: haemostasis phase, inflammatory phase, proliferative phase, and remodelling phase [6],[7]. (See Figure 2 for a summary of the process).

1.2.1 Haemostasis Phase

This phase occurs within minutes of the injury and starts due to the rupture of blood vessels. So, the first step is the vasoconstriction of vessels to avoid bleeding out. Next, platelets stick to the exposed collagen fibres. This activates platelets, which suffer a conformational change and start to interact with each other to form the platelet plug and start to release cytokines and growth factors that will activate the coagulation signalling cascade that will end with the formation of a fibrin clot form where the platelets will keep on secreting growth factors [6], [8].

1.2.2 Inflammatory Phase

Inflammation is a natural response of the organism to fight against tissue damage and occurs also within minutes of the injury. However, the inflammation phase of the wound healing process is said to start around the third day after the injury as this is when inflammatory cells arrive at the wounded site. These inflammatory cells are mainly neutrophils and monocytes. They are involved in tasks of cell debris and bacterial removal. These cells arrive at the injury site guided by growth factors such as platelet-derived growth factor (PDGFs) which is released by the platelets forming the clot [7],[8].

1.2.3 Proliferative Phase

Eventually, monocytes will differentiate into macrophages and will start to release TGF-β1 and TGF-α which in turn stimulate the proliferation of neighbouring epithelial cells from the epidermis. They will undergo epithelial to mesenchymal transition (EMT) to acquire a more fibroblast-like phenotype. This way, they can migrate under the clot to start closing the wound and start re-epithelialization. In parallel due to the TGF-β1 and TGF-α released by macrophages and PDGF-A and -B by platelets, fibroblasts start to migrate and differentiate into myofibroblasts (contractibility is enhanced compared with normal fibroblasts). (Myo)fibroblasts begin the process of wound contraction by extending numerous filopodia and lamellipodia which attach to the ECM network and are then retracted (migration) to promote wound closure [7],[9].

Fibroblasts play another crucial role during the wound healing process: the ECM remodelling by secreting matrix components such as collagen Type III and fibronectin. This ECM remodelling is essential because other cells depend on the ECM state to migrate [6]. Fibroblasts also secrete Vascular Endothelial Growth Factors (VEGFs) and Fibroblasts Growth Factor 2 (FGF-2) that will promote the migration of endothelial cells to start the angiogenesis process which is key to re-establish the blood vessels and allow proper vascularization [10].

1.2.4 Remodelling phase

The remodelling phase (the longest stage), begins when the cells that were used to repair the wound are no longer needed so, they are removed via apoptosis [6],[8]. Once again, fibroblasts play a major role in this phase, the ECM is remodelled to gradually acquire more strength. It can be thought of as the maturation of the ECM laid by the fibroblasts in the proliferation stage. In order to do so, they secrete metalloproteases, to degrade some of the ECM components like collagen Type III, secrete collagen type I, fibronectin concentration is reduced, and elastin is secreted. Fibroblasts also organize these fibres along tension lines so they can cross-link thus increasing the strength of the new ECM [11].

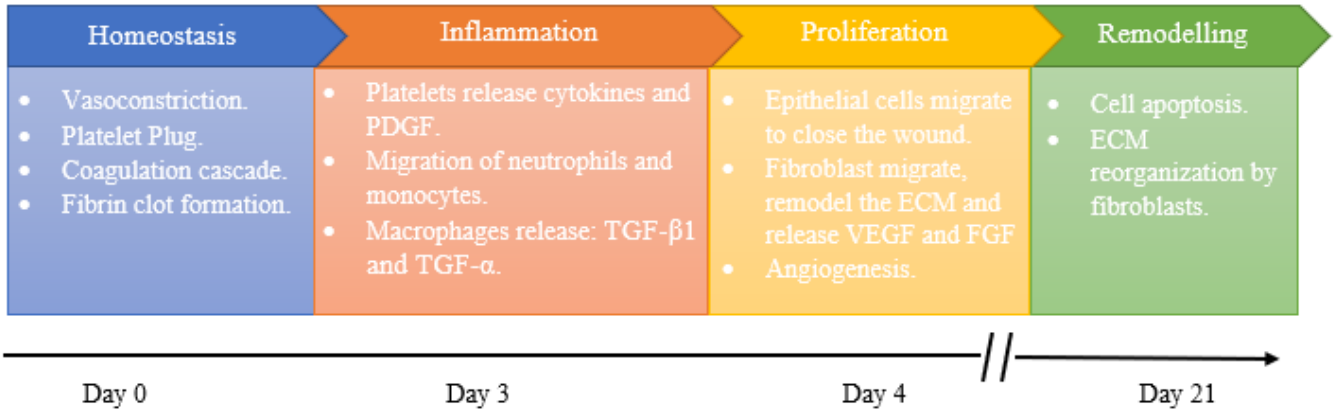

Figure 2: Diagram summarising the wound healing process. The diagram shows each phase of the process, the main events that take place and the approximate moment that each phase starts. Author's figure.

1.3 Extracellular Matrix

The ECM is the largest component of normal skin, a gel-like matrix produced by the cells. It grants fundamental physical scaffolding for the cells and also starts vital biochemical and biomechanical indications that are required for tissue differentiation, morphogenesis and homeostasis [12]. The ECM composition varies between tissues, but it is principally formed by water, fibrous proteins (collagens, elastin, fibronectin, laminins) and proteoglycans. It can be a reservoir for growth factors (GF) and metalloproteases (See Annex A: ***Table 2*** for more information about its composition). ECM changes during wound healing processes and with age [13].

These fibres that make up the ECM can be randomly oriented or form more complex topographies that present two-dimensional (2D) or three-dimensional (3D) guidance cues to migrating cells. Cells exhibit a great array of migration mechanisms (Explained in section 1.4.1) and these are modulated by signalling pathways, intracellular cytoskeleton and adhesion organization in response to physical organization and composition of the ECM [14].

1.4 Fibroblasts

As seen in section 1.2, fibroblasts play a major role during wound healing: they are involved in contracting the wound edges to close it, produce new ECM for other cells to migrate, fibrin clot degradation and ECM remodelling.

Fibroblasts are the resident cell of the dermis layer of the skin which is considered to be connective tissue. All connective tissues contain fibroblasts that accomplish specialized functions and differences in gene expression have been demonstrated between dermal and nondermal fibroblasts [15]. That is why, for this study, we will work with dermal fibroblasts. The migration of fibroblasts is a topic of considerable interest due to its first-hand implication in many physiological and pathological *in vivo* processes such as metastasis of tumour cells during cancer, organ homeostasis and wound healing process.

1.4.1 Migration

As we have seen, cell migration is a vital process in wound healing. It is a multi-step process that leads to the actin-driven translocation of cells on or through a tissue substrate. The most common way to study migration *in vivo* is with two-dimensional (2D) culturing techniques, since compared with three-dimensional (3D) culture, 2D is simple, inexpensive and reproducible. However, fibroblasts under 3D culture conditions, employ different strategies to migrate compared to 2D (See Figure 3). For example, 2D cell migration is mainly directed by lamellipodia and filopodia, whereas 3D cell migration utilizes the formation of filopodia, lobopodia, and blebbing or amoeboid-like movement. These different strategies imply differences in the molecular machinery (protein expression) adopted by cells in 3D and 2D cultures [16].

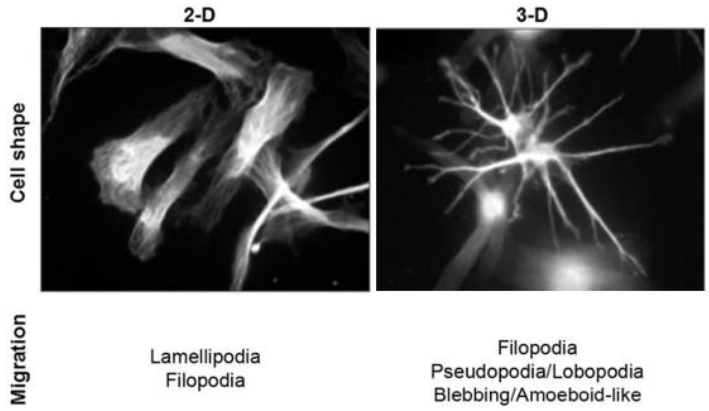

Figure 3. 3D and 2D Differences of Fibroblasts. Fibroblasts cultured on collagen-coated coverslips (2D) spread into an elongated, flattened morphology. Fibroblasts cultured inside of collagen matrices (3D) spread by protrusion of dendritic extension. The main migration strategies are summarized below. Adapted from [16] and [17].

1.4.2 2D Migration Overview

For our experiments, we simply use culture dishes coated with fibronectin thus fibroblasts migrate in 2D. This process can be split into several stages and can be seen as a cyclical process [18] (See Figure 4).

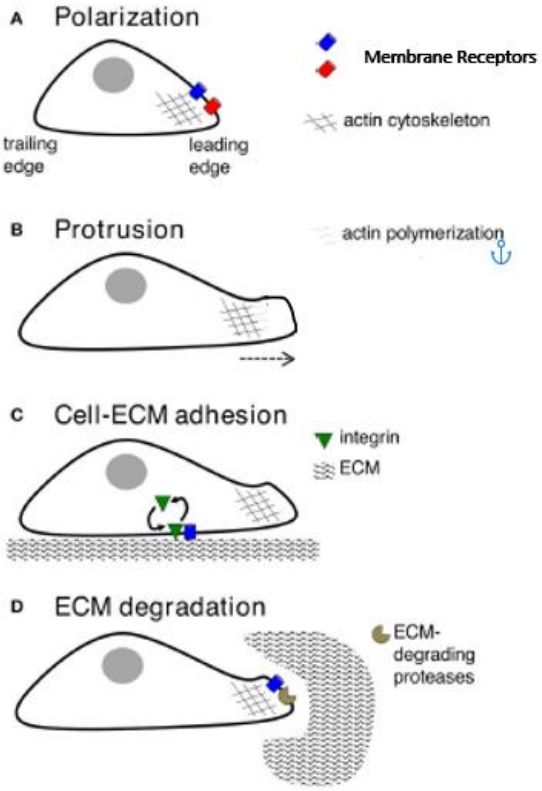

Figure 4: Schematic representation of cell migration. The diagram shows each stage of the process. Figure adapted from [18].

1.4.2.1 Cell Polarization

Cells through membrane receptors are able to respond to external signals such as growth factors, chemokines and cytokines. This leads to the polarization and the extension of a protrusion in the direction of movement. This generates leading edges, regulated by small GTPases, which results in the recruitment of the actin polymerization machinery. Cell polarization enables the creation of specialized domains in the membrane and cytoplasm (protrusions) [18]. (Figure 4 a).

1.4.2.2 Cell Protrusion

By assembling a network of actin filament in the protrusion created in the first step the cell is able to extend its leading edge into the ECM. Protrusions can be classified as lamellipodia, filopodia and invadopodia. Lamellipodia are actin-rich protrusions of 100-400nm of thickness and only have a surface area of few μm^2. Lamellipodia establish contacts with the ECM to which cells adhere. They emit numerous very fine extensions called filopodia, which are used by the cell as a sensing mechanism to explore the environment [19] (See Figure 5). Actin polymerization in response to growth factors and integrin receptor activation is regulated by small GTPases in the Rho family such as Rac1 (lamellipodia) and Cdc42 (Filopodia)[18]. (Figure 4 b).

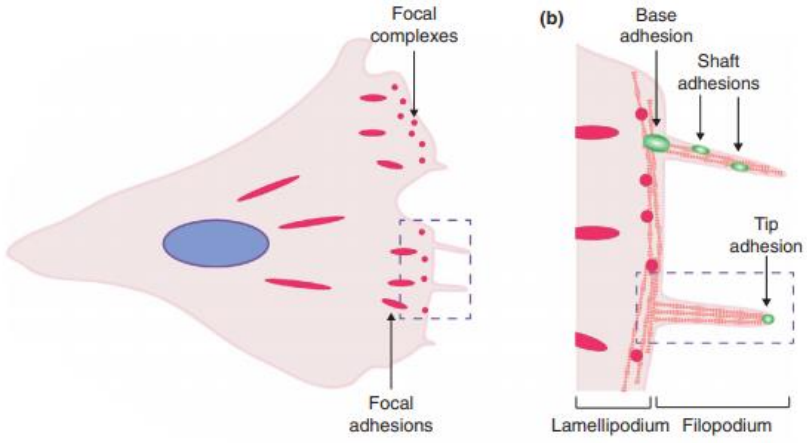

Figure 5. Schematic representation of filopodia during cell migration. Here we can see how lamellipodium elongates from the cell body and filopodium branching out from lamellipodium. Filopodia probe the ECM by assembling specialized adhesion complexes at specific sub-filopodial locations, namely ‘tip adhesions’, ‘shaft adhesions’ and ‘base adhesions’. Figure adapted from:[20].

1.4.2.3 Cell-matrix adhesions

Cells' protrusions interact with the ECM proteins to allow movement via integrin receptors. Integrins, which are transmembrane proteins, link the intracellular cytoskeleton to the extracellular matrix (See figure 6). Integrins transmit information about the substrate to the inside of the cell (outside-inside signalling), thereby providing essential signals for cell migration [21]. This focus of interactions is called 'focal adhesions' (FA) (See Figure). FAs are the anchoring points for cellular forces generated by actin filaments during many biological processes. In FAs, traction is generated by creating enough force to pull the cell forward over the substratum [18]. Integrins reside in FAs through free-diffusion and immobilization cycles (integrin activation promotes immobilization thus, stabilizing FA). (Figure 4 c and 6).

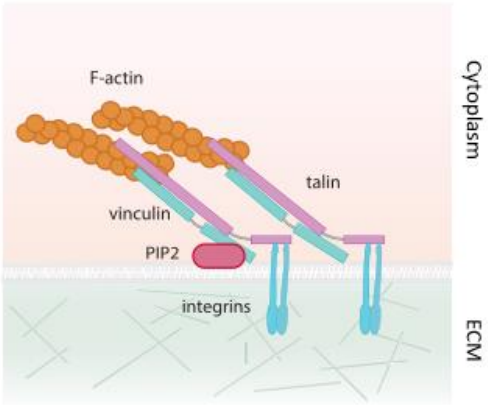

Figure 6. Schematic representation of a Focal Adhesion. Components of focal adhesions and the structures of talin and vinculin when stretched (talin in pink, vinculin in light blue, PIP2 in purple, and F-actin in orange). Figure from: [22].

1.4.2.4 Extracellular matrix degradation

Invadopodia sprouts from filopodia and adhere to the ECM collagen fibres through tiny channels in the ECM. To facilitate the migration of the cell, displacement- impeding ECM fibres are cleared by local proteolysis, using surface proteases like metalloproteinases (MMP). Basically, extracellular matrix degradation widens pathways through which cells can migrate [18]. (Figure 6 b and Figure 7)

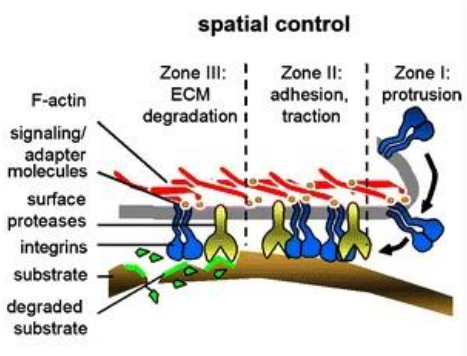

Figure 7: Detailed representation of the protrusion, cell-ECM adhesion and degradation stages in the migration. Figure from [23].

1.4.3 En-masse and single-cell migration

Depending on which tissue they are forming, cells will migrate using different strategies. For example, epidermis cells like keratinocytes are very close together thanks to cell junctions, which makes them migrate collectively. Collective migration is characterised by cells moving while maintaining cell-cell contacts, this is also known as sheet migration [24]. However, due to the dermis characteristics, fibroblasts are not as tightly together as epithelial cells (fibroblasts have fewer cell junctions compared with epithelial). So, they present two other types of cell migration, en-masse migration and single-cell migration (See Figure 8).

En-Masse migration is described when multiple cells are involved, meaning to some extent there is cell-cell communication and also ECM-cell communication [24]. Single-cell migration is very self-explanatory, there is a total lack of cell-cell interaction and there is only ECM-cell communication (integrin-mediated)[24].

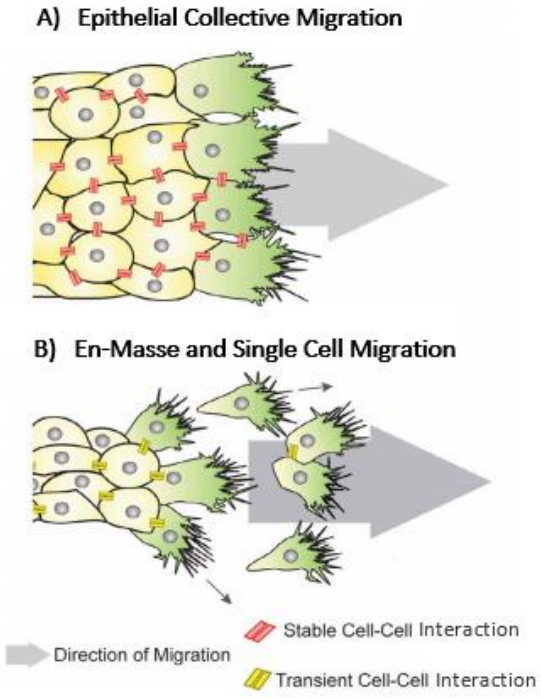

Figure 8: Schematic Representation of different types of cell migration. A) Shows epithelial cell migration, characterised by stable cell-cell interactions (red). B) Mesenchymal cells usually present En-Masse migration characterised transient cell-cell interaction (yellow) and Single Cell interaction which there is only ECM-cell interaction. Figure Adapted from: [25].

1.4.4 Factors Affecting Migration

1.4.4.1 *In Vitro* Ageing

Membrane receptor expression (integrins, growth factor receptors) and post-transductional modification vary not only between different tissue-origin fibroblasts as mentioned in section 1.3 but also according to *in vitro* ageing [26]. This in turn, along with many other factors, affects migration negatively [27]–[29].

It is generally accepted that tracking the population doubling level (PDL) of cells is the best practice for reporting cellular age *in vitro*. The population doubling level is the total number of times the cells in a given population have doubled during *in vitro* culture [30]. It is well documented in the literature that cell morphology, phenotype, cell migration, cytoskeleton organization and actin turn-over can change the more times cells replicate *in vitro*. Young cells (low PDL) grow to higher cell densities at a higher growth rate than aged cells (high PDL) [31] (See figure 9). The culture of mortal cell lines has been used as a model for the aging due to the limited life span *in vitro*. This replicative senescence is proposed to reflect processes that occur in aging of human organs and tissues [31]. (See Annex B, Section 8.3, to see the PDL carried out for the fibroblast used in this study).

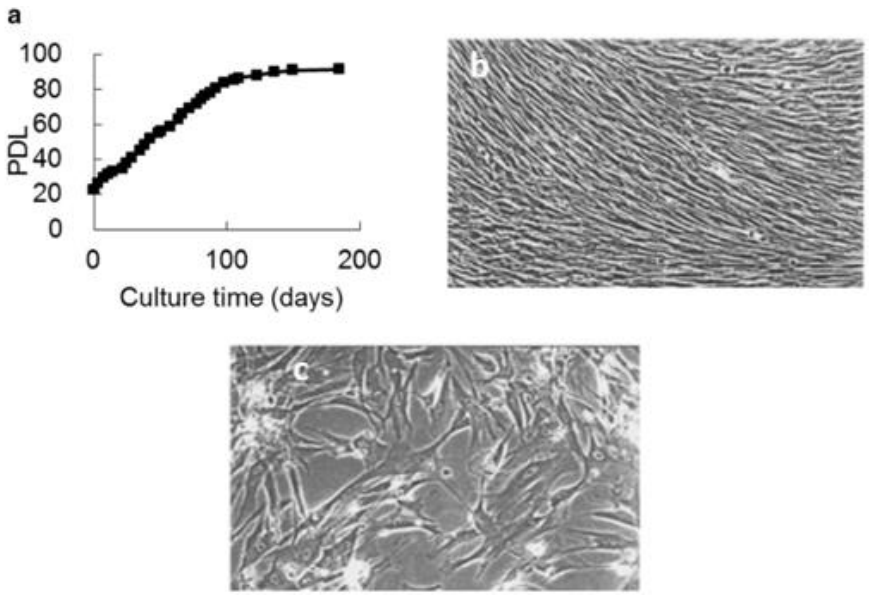

Figure 9: Population Doubling Level. (a) Average proliferation of fibroblasts plotted as PDL for approximately 180 days of culture. (b) and (c) show morphological appearances of PDL 23 (b) and PDL 77 (c). Figure adapted from: [31] and [32].

1.4.4.2 Growth Factors

As we have seen in section 1.2 and will be further be discussed in section 1.6, growth factors are strong mitogenic agents that stimulate the migration, proliferation, and differentiation of cells. There are plenty of studies that prove that growth factors increase the migration rate of cells [33]–[38]. In addition, fibroblast migration in response to growth factors is reduced with ageing [36].

Another thing to consider is that cells *in vitro* are maintained in a medium, which provides energy and substances that help the cell to survive. Many of these substances are added by supplementing the media with Foetal Bovine Serum (FBS). However, the main reason for the addition of FBS is the large amount of growth factors it contains. Usually, cell lines companies like ATCC Cell Lines, recommend keeping fibroblasts in a medium high on FBS (15%) in order to have a high proliferation and migration rate. Recent studies have shown that culturing cells at a high FBS percentage will induce them to differentiate into a tumour-like phenotype (elevated proliferative state and highly migratory abilities). On the contrary, low percentage supplemented FBS medium, allow fibroblast to acquire a phenotype most similar to conditions in the living dermis [39].

1.4.4.3 Extracellular Matrix Properties

The migratory activity of fibroblasts, and other cells, is influenced by the fibres' distribution and assembling of the ECM, which is sensed by integrins. Cells generate significant spatio-temporal deformation of the matrix before and during the migration so that cells on soft matrices migrate along tortuous paths. However, as the matrix stiffness increases, cell migration patterns become aligned with each other and show coordinated migration paths [40].

In vitro studies have been carried out to assess how different ECM proteins affect migration by coating the culture dishes with different concentrations of ECM proteins [41]–[43]. Extracellular matrix composition and fibre orientation are also affected by age [13].

1.4.5 Wound Healing Assay

One of the most well-established methods to study migration and the wound healing process *in vitro* is the "Scratch Assay". The wound is created by scratching a confluent monolayer of cells with a P200 pipette tip [44] (See figure 10). After the wound is performed, the cell monolayer is washed with PBS to remove cell debris that will block migration and fresh media containing a reduced amount of fetal bovine serum (FBS) is added. FBS is reduced to make sure the wound is being closed by cell migration and not cell proliferation. After the new media is added, the cells are recorded and then the images are analysed to calculate the migration rate of the cells [45].

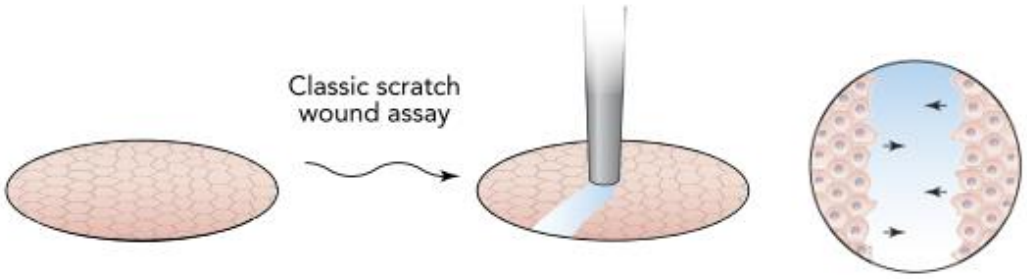

Figure 10. Schematic representation of a classic scratch assay. Figure adapted from [46].

Even though scratch assay is the most common approach due to its inexpensive and easy to implement characteristics, it has some disadvantages [47]. The main one being that the gap-free area is created manually, which means it is difficult to generate reproducible wounds. In addition, applying too much pressure may damage the extracellular matrix, which means cells will migrate over an unphysiological substrate (glass or plastic depending on the culture dish you are working with) this can affect the migration rate [21]. (See Section 1.4.4.3).

Since cell motility is influenced by the interaction of cells with their surrounding matrix, many alternatives to scratch assay have been developed to overcome scratch assay disadvantages. New methods include: thermal, electrical and laser wounding [48]. These options are usually ruled out because they are expensive, and not all laboratories have the means to perform them. A more cost-effective alternative is the solid barrier wounding assay. This migration assay consists of placing a barrier in the culture dish of choice and seeding the cells at both sides of the barrier. This way, once the barrier is removed a free-gap area is created. (See Figure 11)

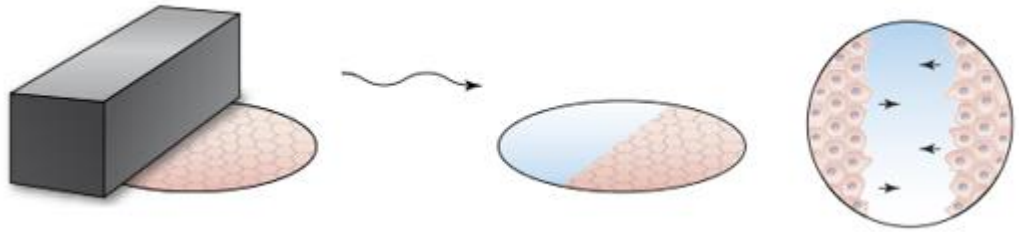

Figure 11. Schematic representation of a wound healing assay using the solid-barrier method. Figure adapted from [46].

Whatever method is chosen to inflict the wound, in order to complete the assay, images are acquired over a period of time to see how cells migrate under different conditions. It is recommended to work with the highest magnification objective that allows you to visualise both sides of the wound and phase contrast imaging or bright field imaging is also advised [46].

Once the images are acquired, using image analysis software such as *Image J*, one can calculate at what rate the cells are closing the wound by measuring the area of the gap along time. When plotted in a graph, the wound healing rate can be calculated by finding the slope of the line [45].

1.4.6 Cell Tracking

In addition, once the images are obtained, tracking of cells can also be done, by doing this more information can be obtained, such as individual cell speed. Cell tracking has become a topic for which interest has expanded in recent years [49].

Nowadays there are many software that allows you to perform cell tracking. The result of the tracking software is a sequence of coordinates indicating the position of each tracked cell at each time point. The first step is to reconstruct the trajectories of the tracked objects from the measured coordinates. Given the trajectories, a variety of measures can be calculated [49]. The most obvious measures of motility include the ‘Mean Square Displacement’(MSD). MSD is a measure of the deviation of the position of a particle with respect to a reference position over time [50] (See figure 12 A). Basically, the MSD can be thought to be the area explored by a particle.

.

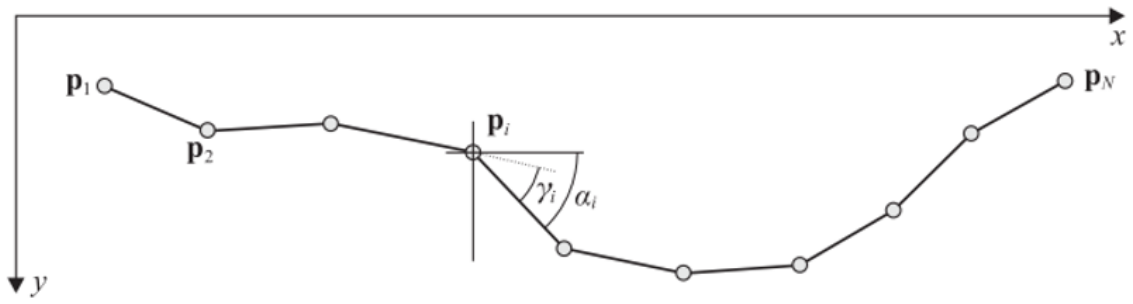

A) $\mathrm{MSD}(n) = \frac{1}{N-n}\sum_{i=1}^{N-n} d^2(\mathbf{p}_i, \mathbf{p}_{i+n})$

B) $v_i = d(\mathbf{p}_i, \mathbf{p}_{i+1})/\Delta t$

C) $\alpha_i = \arctan(y_{i+1} - y_i)/(x_{i+1} - x_i)$

Figure 12. Tracking Equations. The drawing shows a sample trajectory consisting of N points Pi= (xi,yi). A constant frame rate is assumed with a time interval of Δt seconds between successive frames. d(Pi,Pj) is the distance between Pi and Pj. A) Means Square Displacement (MSD); B) Instantaneous Velocity and C) Turning angle. Figure adapted from: [49].

With the MSD one can calculate the diffusion coefficient (*D*) which is determined by fitting the first four points of the MSD curve. This fit is generally used to determine *D* independently of the type of motion [51]. The diffusion coefficient put simple, is a value that represents how easy an object (cell or particle) moves in a given solvent.

Alternatively, the instantaneous velocity (displacement from one frame to the next, divided by the time interval) can also be calculated as a simple way to obtain information concerning the rate of displacement (See figure 12 B). Another interesting value that can be the 'Directional change' also known as 'Turning angle' (See figure 12 C) [49]. By plotting a polar histogram of the angles of the cell's trajectory, we can classify the motion of the cell as random (angles go in many directions) or directed (most angles go in the same direction).

1.5 Integrins

Integrins are heavily glycosylated transmembrane heterodimeric proteins. All 24 integrin-type adhesion receptors are formed by one of the 18 α subunits and one of the 8 β subunits, which interact with each other in a noncovalent manner. Integrins have a crucial role during the migration process. The integrin–ECM binding is used by the cell to determine the microenvironment, a process referred to as mechanoperception. This process directly influences fibroblast's activity by affecting adhesion, receptor expression, gene expression and protein synthesis, as well as influencing the cytoskeleton and cell motility. Integrins provide a molecular link by attaching cells to the ECM [52].

They are composed of an extracellular domain, a transmembrane domain and a short cytoplasmic tail. Extracellular domain subunits have a metal ion-dependent adherent site (MIDAS), crucial for ligand binding[53].

The different combinations of the different alpha and beta subunits give rise to ligand specificity for different ECM components and expression in different cell types. Due to this, they are divided into four different categories: RDG receptors (Integrin $\alpha_5\beta_1$); Collagen receptors, Laminin receptors and Leukocyte-specific receptors (See figure 13).

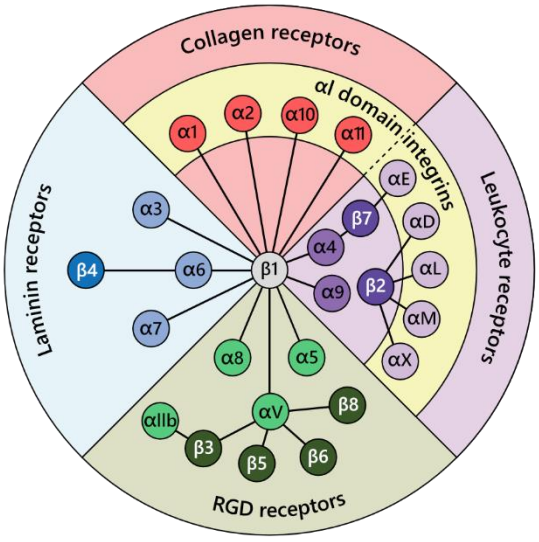

Figure 13: Schematic representation integrin receptor combination. This diagram depicts all 24 integrin subunit pairs, including their ligand specificity for ECM components. Figure from: [54].

It is believed that the integrin α subunit is more involved in the heterodimeric-specific interactions and the β subunit takes part in the interaction with other receptors and signal transduction due to its cytoplasmatic tail which, interacts with tens of signalling proteins [55].

Integrins can be found in three different conformational states in the cytoplasmatic membrane: bent, extended-closed and extended-open (See figure 14). These three states are directly related to the affinity state for their ligand and their signalling mechanism, being the bent state the lowest affinity state and extended-open the state that has maximum affinity[56]. This bent state structure undergoes reversible conformational changes to increase ligand affinity, meaning that these proteins can be activated from the inside by proteins interacting with the cytoplasmic tails (inside-outside signalling), and from the outside by ligand binding (outside-inside signalling) [57].

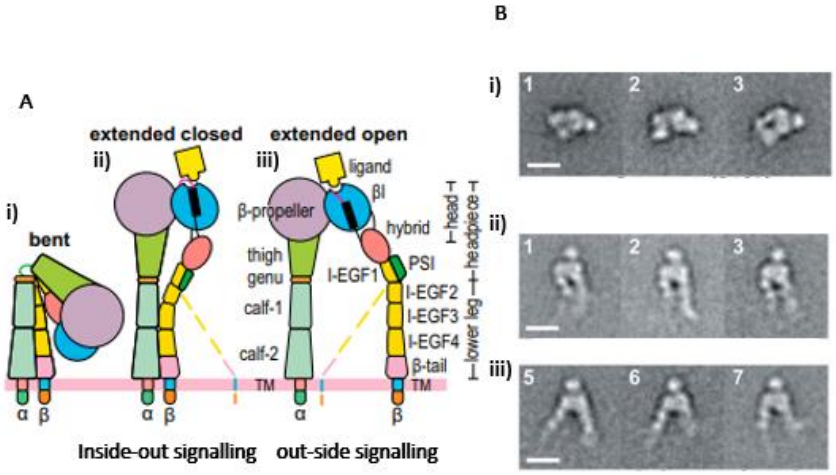

Figure 14: Integrins conformational states. (A) Depicts the three conformational states: i) bent; ii) extended closed and iii) extended open. It also shows the different domains of the α and β subunits. (B) Negative stain electron microscopy images of the state represented in (A). Figures adapted from [56] and [57].

The inside-outside signalling induced by interaction with growth factor receptors (GFR) can be further divided because signal integration between the two receptor systems occurs in many ways. Concomitant signalling: independent regulation of the same pathway; Collaborative signalling: Integrins create a scaffold of signalling proteins and assist in growth factor-dependent signalling in GFR; Direct activation signalling: it has been described that integrins are able to activate GFR in the absence of growth factors; Amplification signalling which implies that GFR-generated signalling may produces the overexpression of integrins, increasing the number of integrins may in turn further activate the GFR signalling; and finally Negative Regulation were GFR signal transduction is inhibited due to phosphatase activation by integrins [27] ,[55].

Diffusion patterns along the plasmatic membrane change also according to the different states of the integrins. The bent conformation due to its inability to interact with any ligand will move freely so, diffusion will be higher (See section 1.5.2, Figure 19). On the contrary, the more active conformations, as the extended-open conformation, will be anchored by the cytoskeleton and other signalling transducing proteins or by interacting with the ECM components. Hence, its diffusion will be reduced (immobile).

1.5.1 Integrin $\alpha_5\beta_1$

This study is centred in the integrin $\alpha_5\beta_1$, fibroblasts express this integrin along with many others. However, integrin $\alpha_5\beta_1$ plays the most critical role *in vivo* during cell migration into the wound [58] . This integrin belongs to the RDG receptors group, which means, it recognises the arginine-glycine-aspartic motif of fibronectin (See figure 15). Fibronectin (FN) is an ECM protein with a multidomain structure, each domain can interact with different integrins and other ECM molecules. It is made up of two similar subunits that are linked in an antiparallel orientation by two disulphide bonds. It is formed by repeating homologous type I, II, and III units. Integrin $\alpha_5\beta_1$ interacts with fibronectin through type III repeat 10 and is the only integrin that interacts with type III repeat 9 [59].

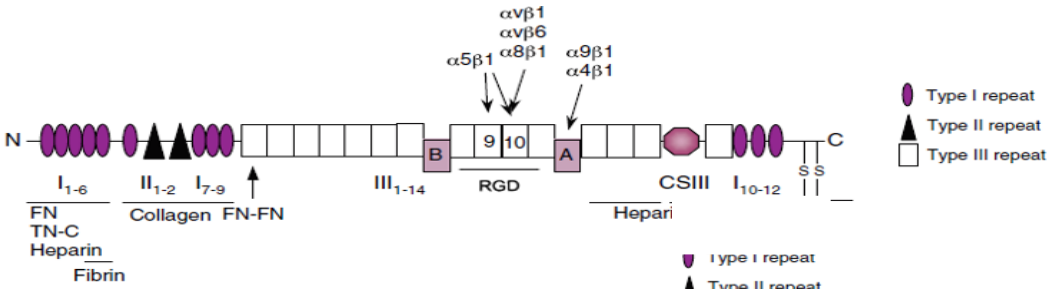

Figure 15: Schematic representation of fibronectin. The figure shows the structure and functional domains of fibronectin. Integrin $\alpha_5\beta_1$ is able to interact via type III 9 and 10 repeating units (RDG). FN has three sites of alternative splicing: type III repeats A and B as well as the CSIII segment. Type I repeat (purple ovals), Type II (black triangles), Type III (white rectangles) Figure adapted from [59].

Integrin $\alpha_5\beta_1$ is heavily glycosylated with 26 potential N-linked glycosylation sites, and it is well known that these glycosylations are involved in the correct integrin-fibronectin interactions as well as integrin-growth factor receptor interactions [60] (See figure 16).

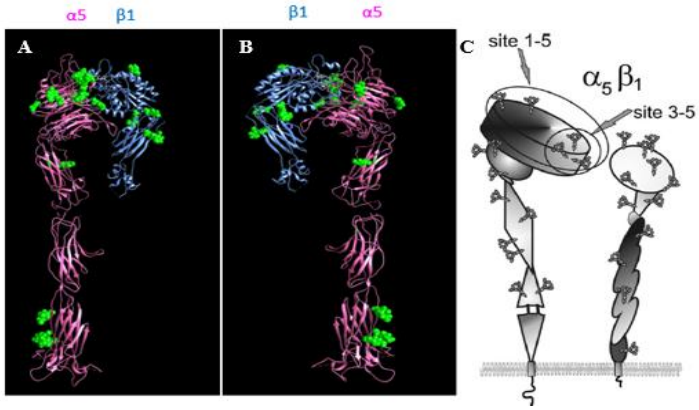

Figure 16. Localization of glycosylation on integrin $\alpha_5\beta_1$. (A) and (B) Ribbon drawing of crystallized $\alpha_5\beta_1$ [shown in pink (α5), blue (β1) and green (glycosylations)], (C) Schematic representation of Integrin $\alpha_5\beta_1$, on integrin $\alpha_5\beta_1$ the 1–5 glycosylation sites were suggested to play a role in heterodimer formation, and on site 3–5 were shown to influence α5β1-mediated cell migration. Figure adapted from [60] and partial crystal structure from PDB: 3VI4 and 4WK0.

1.5.2 Single-Particle Tracking

In summary, integrin-mediated migration and signalling is influenced by its conformation, spatiotemporal organization (diffusion or clustering) and by interaction with other components of the membrane, a technique that allows to study this spatiotemporal organization is single particle tracking (SPT)

SPT has emerged as a powerful approach to study a variety of dynamic processes in life sciences. SPT provides access to single molecule behaviour in the natural context of living cells [61]. SPT is the observation of the motion of individual particles within a medium. The coordinates time series (x, y) or (x, y, z), is called trajectory. The trajectory is analysed using statistical methods to extract information [62] (See Figure 17). In our case trajectory analysis is used to measure the diffusion coefficient.

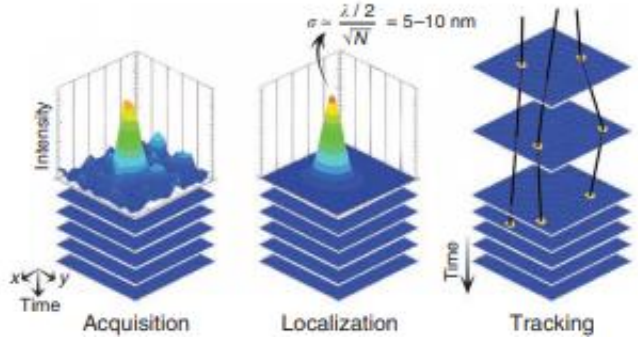

Figure 17. Overview of Single Particle Tracking method. First, images are acquired, which are usually movies composed of frames. Then, the QD or labelling molecule is localized (using characteristics like its diameter). Finally, QD are localized in each frame and their trajectory is obtained. Figure adapted from [63]

The molecules of interest must be labelled with a fluorescent probe so that they can be visualized (See Figure 18 C). The fluorescent label can be a fluorescent protein, a fluorescent dye, or a quantum dot (QD) (See Figure 18 A). The fluorescent label must be conjugated to a biomolecule that binds to the protein of interest. For example, an antibody [64]. If the biomolecule used is an antibody it must be reduced (halved) to avoid inducing artificial clustering while tracking the molecules of interest. (See figure 18 B).

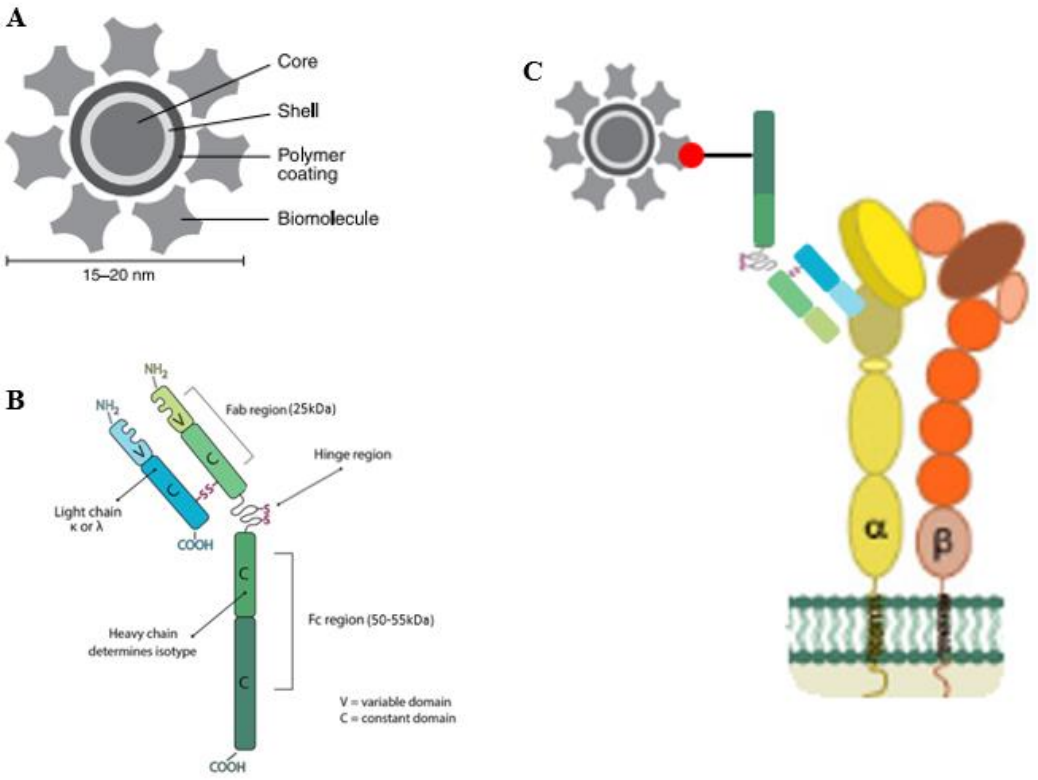

Figure 18: Quantum Dot and half antibody for protein labeling in SPT. (A) Schematic of the overall structure of a Qdot® streptavidin conjugate. (B)Structure of an antibody after the reduction (half antibody -hAb). (C) Schematic representation of a half antibody conjugated with a quantum dot, thanks to a linker molecule, recognising its target protein, in this case, an integrin. Figure adapted from [65] and [66]

For cell membrane SPT studies, the most favourable illumination scheme is based on total internal reflection fluorescence (TIRF) (See Figure 19) [61].

In TIRF microscopy, the excitation beam incidents on the coverslip at an angle such that the beam is reflected and only the evanescent wave enters the sample, exciting only molecules close to the surface [67]. TIRF allows for selective excitation of fluorophores bound to the cell surface, while non-bound molecules are not excited thus, eliminating the background noise (QD out of focus or autofluorescence of molecules inside the cell).

The evanescent waves, which enables this selective excitation, is created when the incident excitation beam is completely reflected from the glass/medium interface. The reflection produces a very thin electromagnetic field in the aqueous medium. This field, the evanescent wave, undergoes exponential intensity decay with increasing distance from the interface allowing the excitation of fluorophores near the surface [68]. (See figure 19).

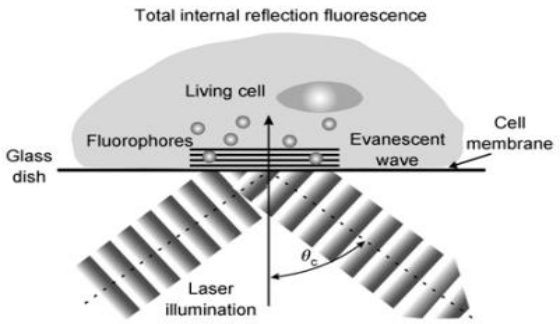

Figure 19: Schematic diagram of total internal reflection fluorescence microscopy imaging of a cell.

After the observation of the motion of the QDs attached to the molecule of interest, the trajectories are reconstructed and analysed to extract information such as diffusion. To assess the diffusion, 'mean square displacement' (MSD) is calculated for each trajectory and the diffusion is the slope of a linear regression fit to the first four points (Figure 11 A).

The MSD values can be analysed by 'Probability Distribution of Squared Displacement' (PDSD) (See figure 20). The PDSD is a statistical analysis that will group the displacement values (MSD) into different modalities (See figure 20 B), where r is the radius; r^2_1 and r^2_2 are slow and fast displacements at different timelags and α is the probability of finding the particle within a radius, meaning the closer is α to 0 the lower the probability of finding the particle out of the radius of confinement (figure 20 i and ii) and the closer α is to 1 the higher the probability of finding the particle far away from the radius of confinement (Brownian diffusion, figure 20 iii and iv), α and 1- α can be seen as a percentage of each type of diffusion modality.

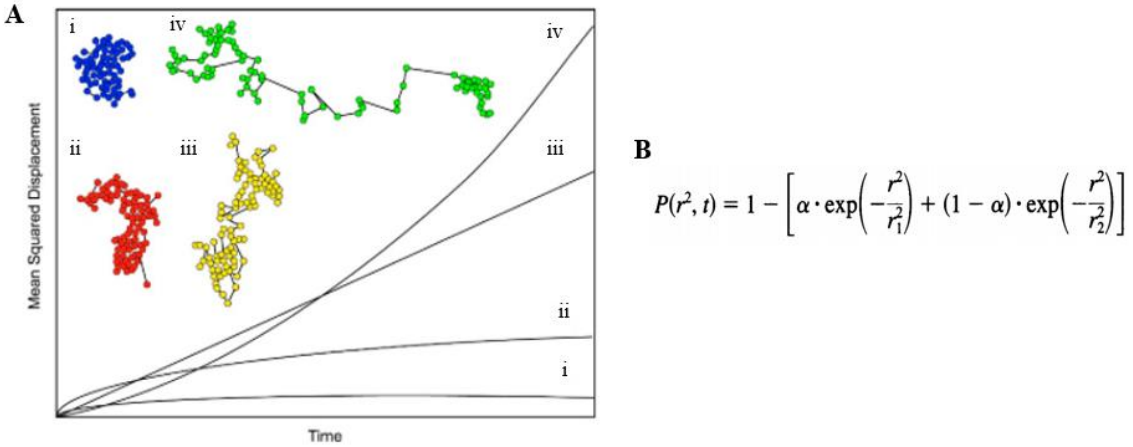

Figure 20: Diffusion modalities and PDSD formula: (A)(ii) Confined molecule motion (slow); (ii) Subdifussive motion; (iii) Brownian diffusion motion; and (iv) free diffusion motion. Their respective MSD plots are also shown. (ii), (iii) and (iv) can also be classified as anomalous (fast diffusion); (B) PDSD formula. Figure adapted from [64][69].

1.6 Growth Factors

As we have seen in section 1.2, growth factors are released since the early beginning of the injury and coordinate the whole process. These proteins released by cells coordinate many physiological processes. When they interact with their receptor, a signal transduction cascade is started and usually ends with the activation of a transcription factor that will give rise to the transcription of a gene that will carry out a function related to a biological process such as, proliferation, differentiation and migration. The principal growth factors involved in wound healing are depicted in figure 21 and summarized in ***table 3*** (See Annex A).

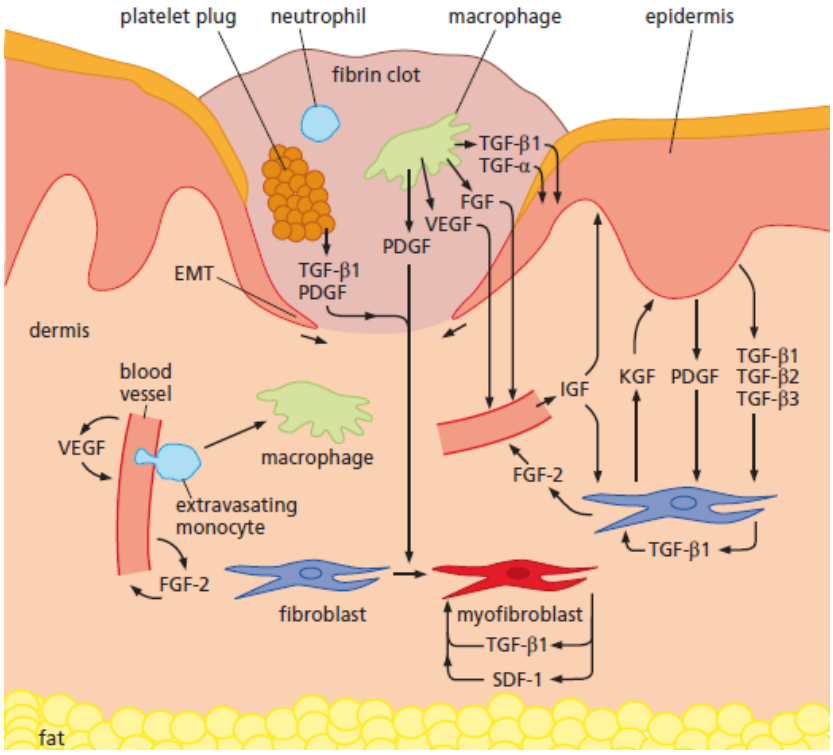

Figure 21: Wound Healing Program: The diagram depicts the heterotypic growth factor signalling occurring after the skin is wounded. Figure from: [10]

It should be said that growth factors function, cell source and target cells are in constant actualization. This means that not all the functions and target cells are reflected in figure 21 nor ***table 3***.

In the last decades, growth factors have been used as a treatment to improve the wound healing process. The most popular between those treatments is the platelet-rich plasma therapy (PRP) [70]. PRP is defined as a portion of the plasma fraction of autologous blood having a platelet concentration above baseline. This treatment has gained popularity because, as we have already seen, platelets are one of the key producers of growth factors during the wound healing process [71]. The growth factors released and their quantity depend on the patients, but the principal growth factors released are PDGF (0,25 ng/ml); EGF (7,9 ng/ml); TGF-β1(62ng/ml) and the most abundant on average, VEGF (20ng/ml) [72].

1.6.1 Vascular Endothelial Growth Factors (VEGF) and its Receptors

The Vascular Endothelial Growth Factor (VEGF) and its receptors (VEGF-R) are key regulators of angiogenesis (a crucial step for wound healing) and endothelial cell migration, proliferation and survival. The VEGF family is composed of VEGF-A, PGF (placenta growth factor), VEGF-B, VEGF-C, VEGF-D and VEGF-E which can interact with its receptors, VEGF-R1, VEGF-R2 and VEGF-R3. VEGF-R1 has a soluble isoform which lacks the transmembrane domain. Neuropilins (NRPs) are co-receptors for VEGFs and they work by increasing the affinity between VEGF and its receptors [2]. (See figure 22).

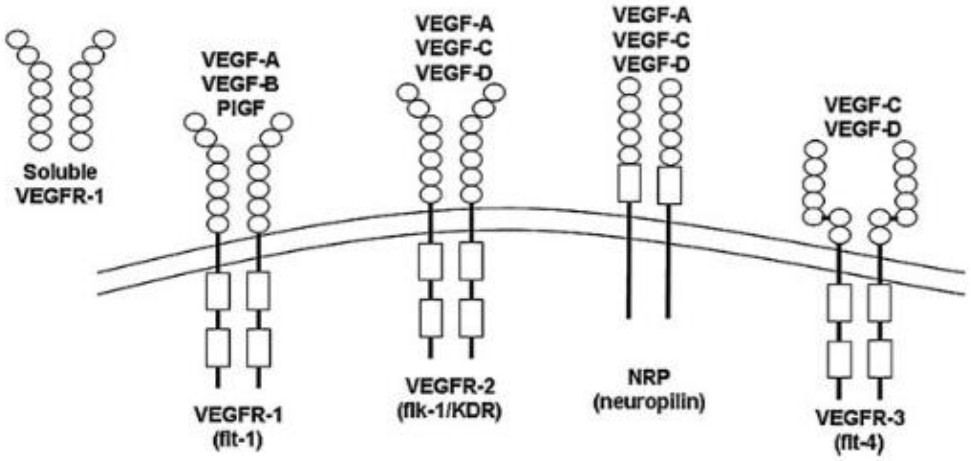

Figure 22: Schematic representation of Vascular Endothelial Growth Factor Receptors. The picture shows the different VEGF-Rs and its different ligands. Figure from [2].

Due to their name, one may think that only endothelial cells express VEGF-Rs and are the only cells that are able to respond to VEGF, but this is not the case. There is not much research in this field, but some studies have been carried out on the expression of VEGF-Rs and the effect of VEGFs on non-endothelial cells [2], [73]–[76]. Human dermal fibroblasts, in particular, express only the VEGR-1 [77].

2. Hypothesis and Objectives

This final degree project aims to study the effect of vascular endothelial growth factor on integrin $\alpha_5\beta_1$ in human dermal fibroblasts in the context of wound healing.

Hypothesis 1: Due to fibroblast expression of integrin $\alpha_5\beta_1$ and VEGF-R1, we believe that integrin $\alpha_5\beta_1$ and VEGF-R1 will directly or indirectly interact with each other.

- Objective 1.1: Gather bibliographical and Protein-Protein Interaction Database information to find out if there is a possible direct and/or indirect interaction between integrin $\alpha_5\beta_1$ and VEGF-R1.

Hypothesis 2: Collective and individual migration rate of VEGF-A treated fibroblasts will increase compared to untreated fibroblasts.

- Objective 2.1: Design a non-damaging extracellular matrix biocompatible solid barrier to perform wound healing assays.

- Objective 2.2: In order to use cell migration to assess the effect of VEGF-A treatment, a pipeline for cell tracking and trajectory analysis must be created. To do so, a tracking software must be chosen and how the results of the tracking software are going to be analysed must be decided.

Hypothesis 3: Integrin $\alpha_5\beta_1$'s diffusion pattern will change upon VEGF-A treatment on fibroblasts.

- Objective 3.1: Find a suitable antibody against VEGF-R1, for tracking experiments, the binding site of the antibody to the VEGF-R1 must be identified to make sure it does not block the interaction with VEGF-A.

- Objective 3.2: Reduce antibodies for Single Particle use and conjugate them with quantum dots.

- Objective 3.3: Assess changes in diffusion pattern of integrin $\alpha_5\beta_1$ with VEGF-A treatment using Single Particle Tracking methods
-

3. Methodology

3.1 Protein-Protein Interaction Data Bases and Networks

To find out any previous described interaction between integrin $\alpha_5\beta_1$ and VEGF-R1, direct or indirect, we carried out a bibliographical research using PubMed and open-source Protein-Protein Interaction (PPI) databases such as *VisANT* (http://www.visantnet.org/visantnet.html) and *IntAct EMBL-EBI* (https://www.ebi.ac.uk/intact/). These databases draw information out from the literature and allow us an interactive and visual way of mining biological interaction of data sets.

3.2 Matrix-Dependent Wound Healing Assay

VRW confocal culture dishes (35mm) with a 20 mm glass centre diameter, were coated with 4mg/ml fibronectin and then blocked with 2mg/ml bovine serum albumin (BSA), washed with phosphate-buffered saline (PBS). Then the solid barrier was placed in the coated culture dish and then primary-dermal fibroblasts (HFF-1 ATCC® SCRC-1041™) were seeded at a concentration of $3.2x10^5$cell/ml with Thermofisher DMEM medium supplemented with 15% FBS,1% of penicillin, 1% of streptomycin and 1% glutamine. After 24h the monolayer is washed and medium containing only 0.5% FBS was added (other supplements were kept the same as described for the 15% FBS medium). Once the cells reach 100% confluency, the solid barrier was removed, the media was washed with PBS and changed for a medium containing the same composition as 0.5% FBS plus 20ng/ml of VEGF-A (Sigma-Aldrich), for the control fresh 0.5% FBS medium was added. Culture dishes are placed under the microscope and movies of migrating fibroblasts are recorded(See section 3.2.3).

3.2.1 Solid Barrier Design

We decided to assess fibroblast migration using the solid-barrier wound healing assay. To do so, we 3D printed the solid barrier using the "Form Labs +1" 3D printer. The barrier was design using *PTC Creo Parametric* 5.0.4.0 software. After the 3D printed barrier is cured (cleaned twice with isopropyl and 45 minutes under UV light) it is cleaned with soapy water for 24h and coated with PDMS (SYLGARD™184 Silicone Elastomer). PDMS is a mineral organic polymer of the siloxane family used due to its biocompatibility properties [78]. The barrier was designed to fit the culture dish we use and to produce wounds of around 0.9 mm wide.

3.2.2 Matrix Damage Assay/ Glycosylation staining

To evaluate the damage produced to the fibronectin coating, we decided to stain the coated dish after the solid barrier was removed. We used 200µl of a 50µg/ml Concanavalin A-Alexa Fluor™ 488 Conjugate (Thermofisher) solution per culture plate. Concanavalin A binds to glycosylation found in fibronectin and fibroblast cell membrane. To assess if the wounds produced by the solid barrier

were uniform the ‘plot profile line’ of the image was acquired using *Image J*. The graph displays intensities of pixels within the image.

3.2.3 Image Acquisition and Microscope Settings

We use a Leica DMi8 inverted microscope, this microscope is equipped with image acquisition software and an environmental chamber (Okolab) equip with temperature sensors (keeps the temperature constant at 37ºC and CO_2 levels at 5%) which allow us a certain degree of automatization.

Once the culture plates are position inside the chamber, we use the spiral acquisition image option to locate the plates on the chamber and calibrate the distance between each plate, this way the microscope software knows where each plate is. Then, we select regions of interest (ROIs). In our case, ROIs are areas where we can see the “wound” and also the cells at both sides. Afterwards, we manually focus each ROI. Fibroblast change size and shape while migrating so, we need to focus using the Z stack option to avoid having blurry images (non-focused). Now we set the software to trigger image acquisition at regular times intervals every 30 minutes for 48 cycles (24h) for each ROI.

3.2.4 Cell Tracking set up

After images are acquired, we used the software *Image J* to pre-process de images, in particular, we used the filter ‘variance’ to highlight the edges of the cells and then the contrast and brightness of each image were adjusted.

Afterwards, the *Ilastik 1.0* software [79] was used to track cells. First, an *Ilastik* pipeline is implemented to segment the raw images, this allows the software to differentiate between background and foreground (cells). This pipeline is called “pixel classification” and its output is a probability map file. This output file along with the raw images are used as an input for the “manual tracking” pipeline, used to track cells. This pipeline output is an HDF5 file.

For further analysis, Dr. Carlo Manzo created two Matlab scripts, the first one, called “main_get_and_refine_traj” reconstructs the tracks from the HDF5 files and allow us to manually correct trajectories by manually adding missing cell localizations, joining tracks or fixing ambiguous reconnections. Finally, the script creates a *Matlab* file called “test_TR_refined” with the x and y coordinates of each cell, the frame of said coordinates and the track identification. The second script uses the “test_TR_refined” file and calculates the MSD, diffusion coeffcient ,the instantaneous velocity and the turning angle for each trajectory.

3.3 Single Particle Tracking Assay

We used single particle tracking (SPT) experiments to investigate the changes in the diffusion pattern of integrin $\alpha_5\beta_1$ with a 20ng/ml VEGF-A treatment at the single molecule level. (See section 1.5.2)

3.3.1 Antibody Selection

For this study, we need to use antibodies that do not block integrin $\alpha_5\beta_1$ interaction with its fibronectin or VEGF-R1 interaction with VEGF-A. The following criteria were used for the antibody selection:

- If their binding site was not clearly stated in the manufacturer's web site, they were immediately ruled out.
- Antibodies that bind to intracellular domains of the receptors were excluded.
- The antibody had to be monoclonal to avoid cross-reactions with other proteins.
- That it could be used for several experimental procedures (western blotting for example) not only for SPT.

Finally, the domain that the antibody targets was visualised using the UCSF Chimera visualization software, to make sure it did not block the interaction site. The best choice was SY09-09 antibody for VEGF-R1 which binds to D1 domain (See Annex A, ***table 4*** for the list of antibody candidates against VEGF-R1). For integrin $\alpha_5\beta_1$ SPT experiments we used the 555651 antibody which targets the α_5 integrin subunit.

3.3.2 Antibody Reduction

For the reduction of the antibody (hAb) (See Figure 18 B) we use 1,4-dithiothreitol (DTT) at 1mM which reduces disulphide bonds (S-S) to sulfhydryl group (-SH) in peptides and proteins [80]. Afterwards 2-Iodoacetamide (IAA) at 20mM excess is added. IAA is an alkylating agent that binds covalently with the sulfhydryl groups. This means that the antibody cannot form back the disulphide bonds [81]. To check if the antibody has been reduced to the desired conformation, we run an 8% SDS-PAGE electrophoresis gel (See Annex B, Section 9.1).

3.3.3 Half Antibody and QD Conjugation

To conjugate the reduced antibodies to the QDs, we used the Qdot™ 655 Streptavidin Conjugate (Q10121MP) form Thermofisher with the emission maximum near 655 nm, it is conjugated with streptavidin (See figure 18 A). First, we need to add an EZ-Link Sulfo-NHS-LC-Biotin linker (Thermofisher) to the reduced antibody. The EZ-Link Sulfo-NHS-LC-Biotin linker (EZ-link) enables a simple and efficient labelling of antibodies or any molecule that contains an amine group [82]. So, the EZ-Link Sulfo-NHS-LC-Biotin linker with one of its extremes will bind to the antibody and the other extreme that contains a biotin molecule will bind to the streptavidin conjugated QD, biotin is a vitamin that will bind with high affinity to streptavidin proteins.

Each streptavidin has four union sites for biotin so, careful attention must be taken to the stoichiometry. We want to achieve a ratio of 1QD:1hAb, for this, it is necessary to add to the reaction a higher proportion of biotin, to fill the majority of streptavidin's biotin binding site and avoid two or more QD per hAb. (See Figure 18 C).

To achieve this, we used 10 mmol excess of a 10 mM solution of EZ-Link Sulfo-NHS-LC-Biotin linker to label each antibody (555651 and SY09-09) and incubated them for 2 hours at room temperature. Then we need to generate three solutions of 200µl 6% BSA PBS each. The first one will contain 20nM of the EZ-link reduced hAb; the second one 200nM of biotin and the third one 20nM of Qdot™ 655 Streptavidin Conjugate. The three solutions are mixed and left in a shaker for 2 hours at 4ºC. The mixture can be stored at 4ºC for no more than 15 days.

3.3.4 SPT Image Acquisition

The cells are seeded in six different coated culture dished (explained in section 3.2). At 70% confluency, cells are washed with PBS and medium containing 20ng/ml VEGF-A is added to 3 out of the 6 seeded dishes, to the other 3 dishes medium containing 0.5% FBS was added (control samples). After 6h the medium is changed for a medium containing a 1/50 dilution of the hAb conjugated with the QDs. After 15 minutes of incubation at 37ºC, the medium is removed, and cells are washed three times with PBS containing Mg^{+2} and Ca^{+2} (to avoid cells lifting), then for better visualization 500µl 6%BSA PBS is added and the culture dish is placed under the microscope.

The microscope is set to the TIRF configuration with the 100X objective (immersion oil is required) and movies of 40 frames per second with a total of 500 frames per movie are created. Subsequently, this movie will be analysed to obtain the integrin $\alpha_5\beta_1$ trajectories and diffusion coefficient.

3.3.5 Localization Precision

For the SPT trajectory analysis first, we need to calculate the localization precision parameter of the equipment. This parameter is used to distinguish between real movement and movement produced by the external vibration of the environment. To calculate this value, we fixed QD on glass culture dishes and record them. After calculating their diffusion, as explained in section 3.3.7. A histogram of the diffusion values was plotted and the percentile 95 was calculated (Annex B, Section 9.4). This value will be applied to every diffusion experiment, to distinguish between real movement from intrinsic vibration (thermal noise).

3.3.6 Trajectory Analysis

The aim of SPT image analysis is to segment and follow over time the labelled protein. So, the TIRF movies were analysed with *TrackMate* v5.2.0, an *ImageJ* Fiji plugin [83]. Each quantum dot is segmented in multiple frames and its trajectory is reconstructed (x and y coordinates are plotted). These tracks can then be analysed to calculate their diffusion.

To analyse the movies the following parameters were used:

- Estimated blob diameter: 0,350 microns.
- Simple LAP tracker.
- Linking max distance: 0.900 microns.
- Gap-Closing max distance:2.5 microns.
- Gap-Closing frame gap: 3.
- Number of Spot in Track: minimum 20.
- Number of gaps in Track: maximum 3.

These parameters are for integrin $\alpha_5\beta_1$, they were calculated using previous published results [84] , for other proteins these parameters should be adjusted.

After the reconstruction of the trajectories, we manually checked each trajectory and eliminate faulty ones. A trajectory is ruled out when two or more QD come across each other's path. Then TrackMate produces a CSV file that contains a track identification number and the corresponding trajectory coordinates for each frame.

To analyse the tracks, we used a *Matlab* script written by Dr. Carlo Manzo and colleagues called '*CPD only*'. The *CDP only* script uses as an input the *TrackMate's* CSV file. The analysis consists of two parts: first, the MSD and diffusion coefficient are calculated for each trajectory. Then, the diffusion coefficient is analysed by 'probability distribution of squared displacement' (PDSD) to find out the best way to classify the different trajectories. So, the '*CPD only'* to perform these two analyses needs the localization precision value, the time between frames and what type of classification we want to do. In our case we classified the trajectories in two groups: confined (slow) or anomalous (fast) which are the most common. So, the result will be the total number of curated trajectories divided into three diffusion categories: immobile (their diffusion value is under the localization precision value); confined in a small region (slow diffusion) and anomalous (fast diffusion).

3.4 Statistical Analysis

After evaluating the normality distribution and homogeneity of variances of the cell tracking data a Wilcoxon signed-rank test statistic test was performed. To analyse the diffusion trajectory classification a Pearson's chi-squared statistic test was used.

4. Results

4.1 Protein-Protein Interaction Data Bases: Integrin α5β1and VEGF-R1

Due to the relevance of integrin $\alpha_5\beta_1$ and VEGF-R1 in the context of wound healing and previous reported interactions between integrins and growth factor receptors we wanted to collect as much information about $\alpha_5\beta_1$ and VEGF-R1 direct or indirect interactions. Therefore, we did a bibliographical and protein-protein interaction database search.

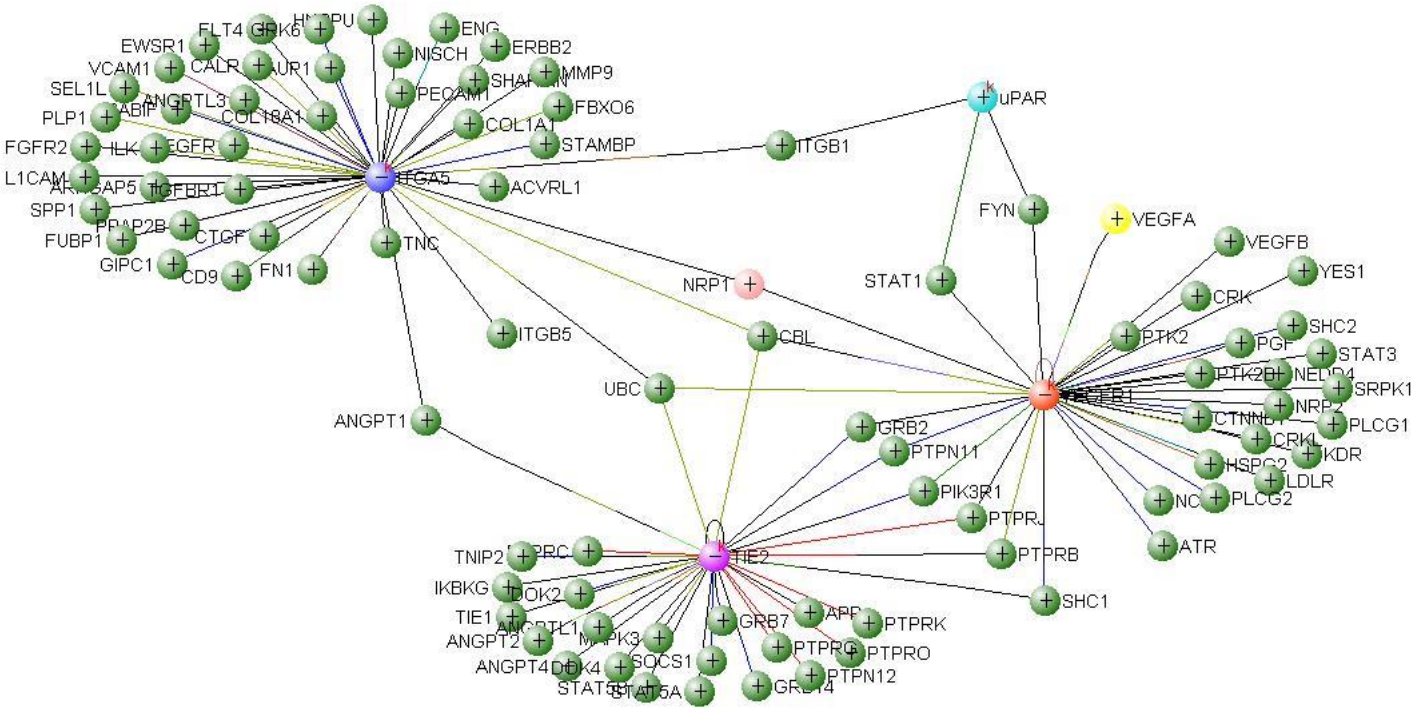

Figure 23: VisANT PPI network for integrin α5β1 and VEGF-R1. The image shows the interaction network provided by VisANT. Nodes represent proteins and edges (lines that connect nodes) depending on their colour represent different methods by which the interaction between proteins has been evaluated. Nodes: dark blue $\alpha_5\beta_1$ (ITGA5); red VEGF-R1; pink NRP1; purple TIE2; light blue uPAR and in yellow VEGFA. Edges: blue yeast two hybrid; light blue coimmunoprecipitation; green affinity technology; chromatin immunoprecipitation red and in black several experimental procedures such as far western blotting and pull-down assay. The network was accessed on the 14th of February 2020.

4.2 Solid Barrier Wound Healing Assay

4.2.1 Solid Barrier Design

To achieve, uniform, reproducible wounds and do not damage the fibronectin coating we design a solid barrier to perform wound healing assays. A total of fifteen different barriers where made. Eleven out of those fifteen were purely made from PDMS, negative moulds of the barrier were printed and the PDMS was poured over them, (See Annex B, Section 9.5). Four out of the fifteen barriers were directly 3D printed as shown in Figure 24 and coated with PDMS as explained in Section 3.2.1

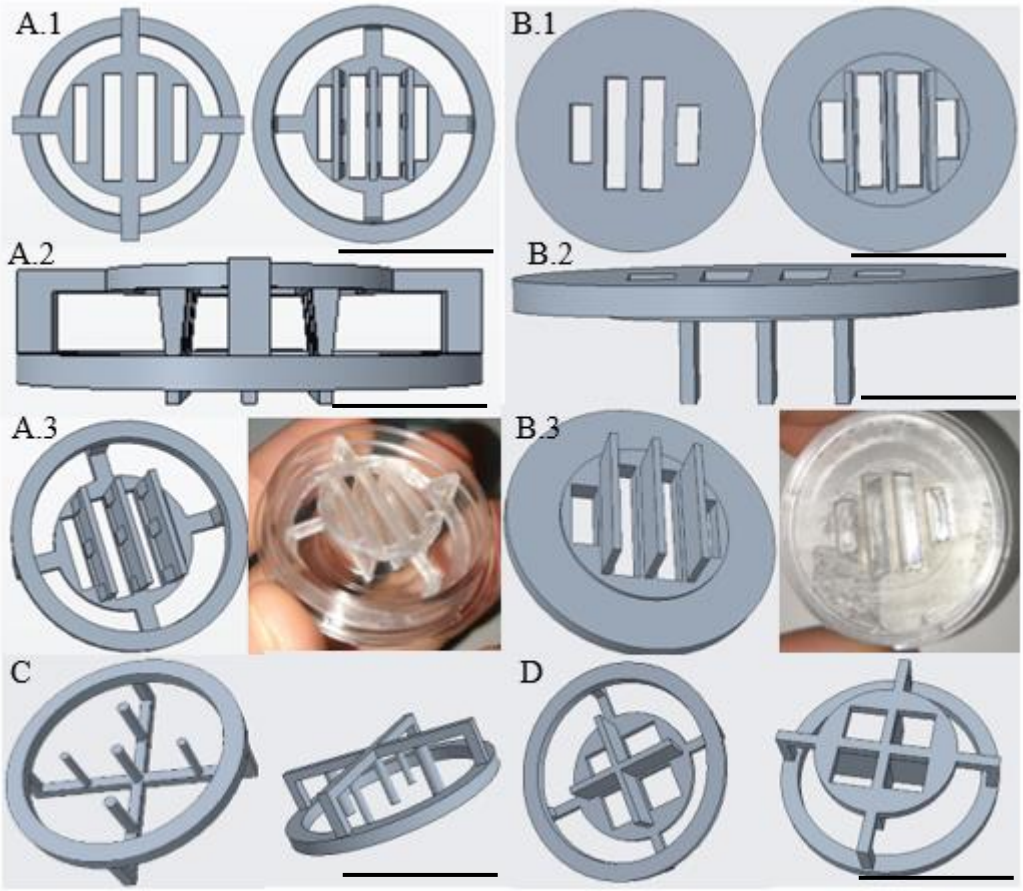

Figure 24: Solid-Barrier Devices. (A) *PTC creo* designs of a solid barrier that secures itself by the bottom part of the culture dish. A.1 Top and bottom view; A.2 Side view of the device; A.3 Another perspective and the 3D printed barrier inside the culture dish. (B) PTC creo designs of a solid barrier that secures itself by the top part of the culture dish. B.1 Top and bottom view; B.2 Side view of the device; B.3 Another perspective and the 3D printed barrier inside the culture dish. (C) PTC creo design of a solid barrier that produces rounded wounds. (D) PTC creo design of a solid barrier that produces cross-shaped wounds. Scale bar 7,8mm.

4.2.2 Matrix Damage Assay/Glycosylation Staining

Before using them for any experiment, we wanted to visualize the wound created by our solid barrier and assess the damage inflicted to the fibronectin coating, In order to do this, we stained the cells and the coating with Concanavalin A-Alexa Fluor™ 488, which binds to glycosylations on the cells membrane and fibronectin coating. The glass is not stained with concanavalin this way we can assess if the coating is removed by the solid barrier.

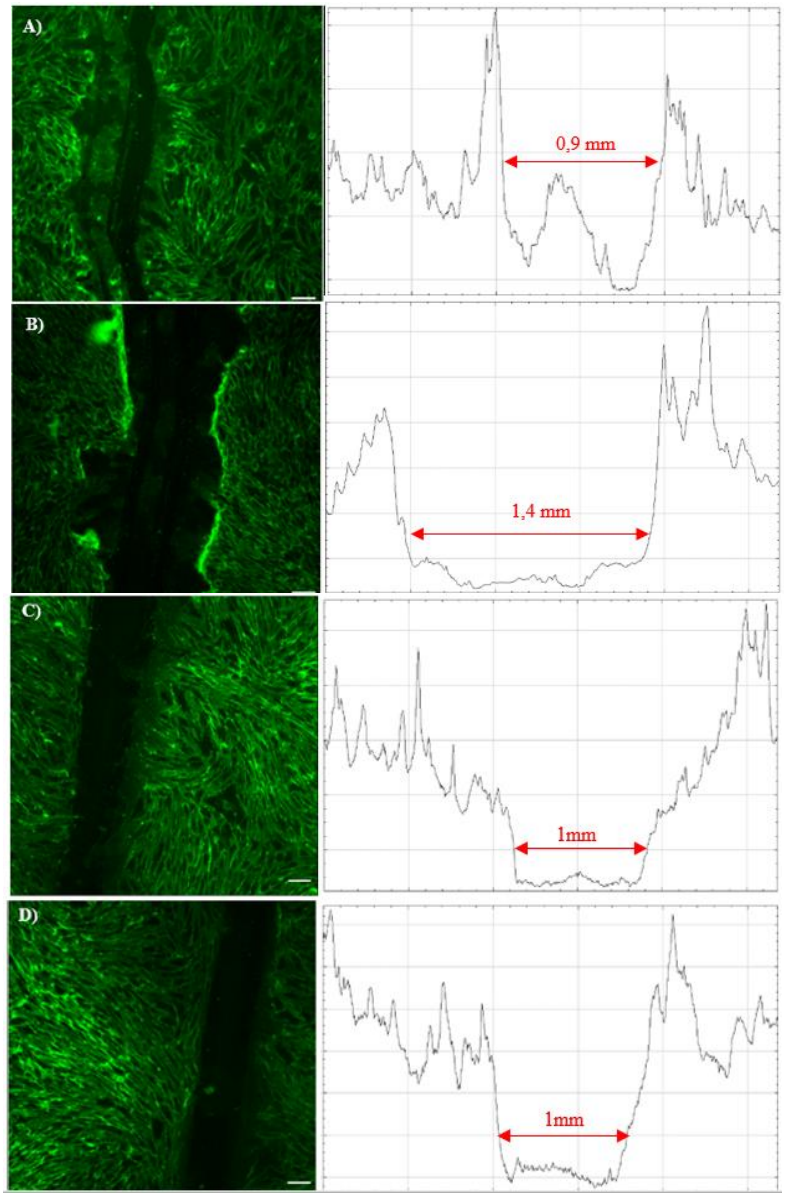

Figure 25. Wound Healing Assay on Human Dermo. Fibroblast on fibronectin/BSA coating stained with Concanavalin A-Alexa Fluor 488. Epifluorescence images were taken at 10x. (A) and (B) representative images of wounds produced by the "Scratch" method using a P200 micropipette tip. (B) and (C) representative images of wounds produced by our solid barrier. Next to each image, there is their corresponding plot line graph, the size of the wound is indicated in red. Scale bar 100µm.

4.3 Cell Tracking

To further evaluate the outcome of VEGF-A treatment on fibroblasts, in addition to the wound closure rate, we wanted to calculate cell velocity, diffusion and direction as an indication of the effects of VEGF-A. To do so, first we had to implement a cell tracking pipeline and decide which was the best software for tracking cells. To decide which software to use we track cells form images we had from fibroblasts growing with 15%FBS culture medium that we used to make sure the environmental chamber of the microscope worked correctly. Once we had decided which software to use, we track fibroblast under 20ng/ml VEGF-A treatment

4.3.1 Cell Tracking pipeline results

Table 1 Summary of Tracking Software. The table shows the number of trajectories that were obtained analysing the same images with each method, the average trajectory length and how time-consuming each method was.

Tracking Method	Number of Trajectories	Average Trajectory Length (38 max)	Time Consuming
Image J Manual Tracking	40	36	Low
Ilastik Automatic Tracking	36	26	Medium
Ilastik Manual Tracking	23	15	Medium
Ilastik Manual Tracking + Matlab	29	35	High

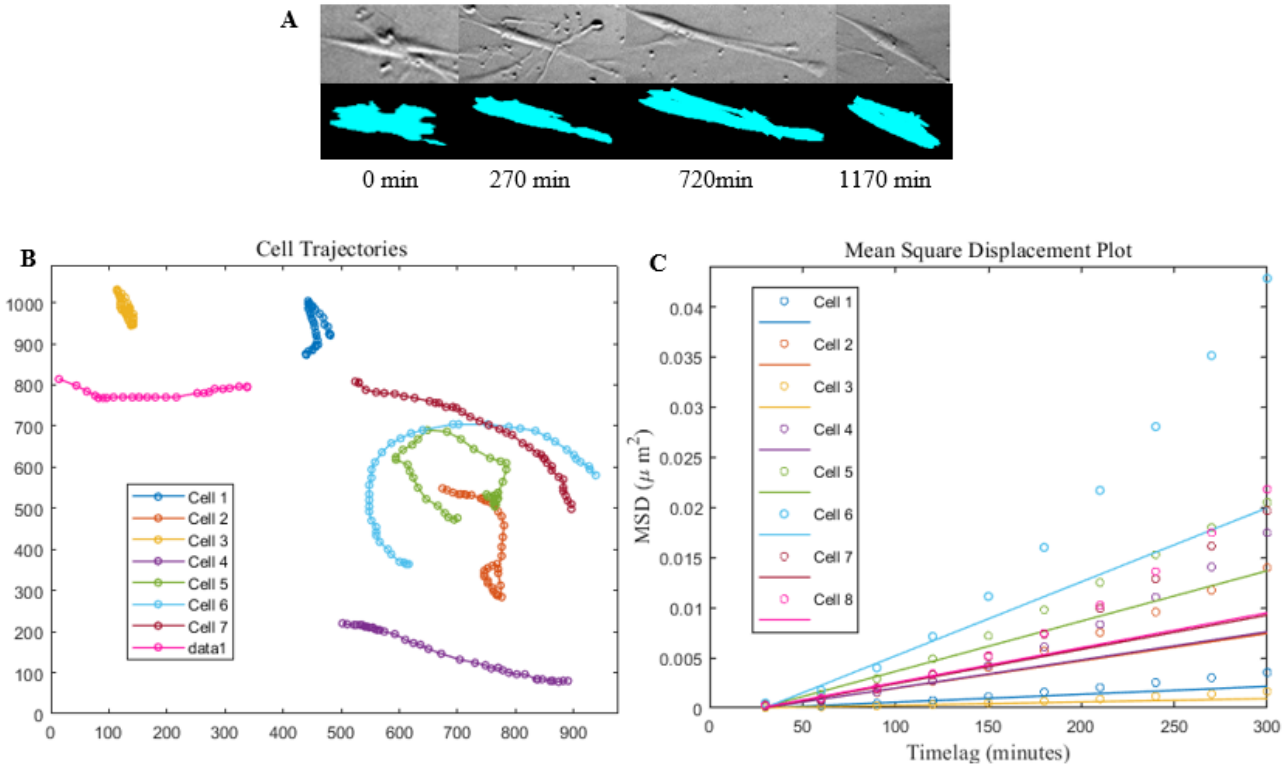

Figure 26. Summary of Cell Tracking. (A) Show the result of the image segmentation, top bright field images bottom: object of the cell in the bright image created based on the segmentation step previous to cell tracking. (B) Shows the reconstruction of the tracks that later on are used to calculate the diffusion, instantaneous velocity and turning angle. (C) Shows the MSD plot of the trajectories shown in (B) the fit is done on the first 4 values (diffusion coefficient).

4.3.2 Cell Tracking under VEGF-A treatment

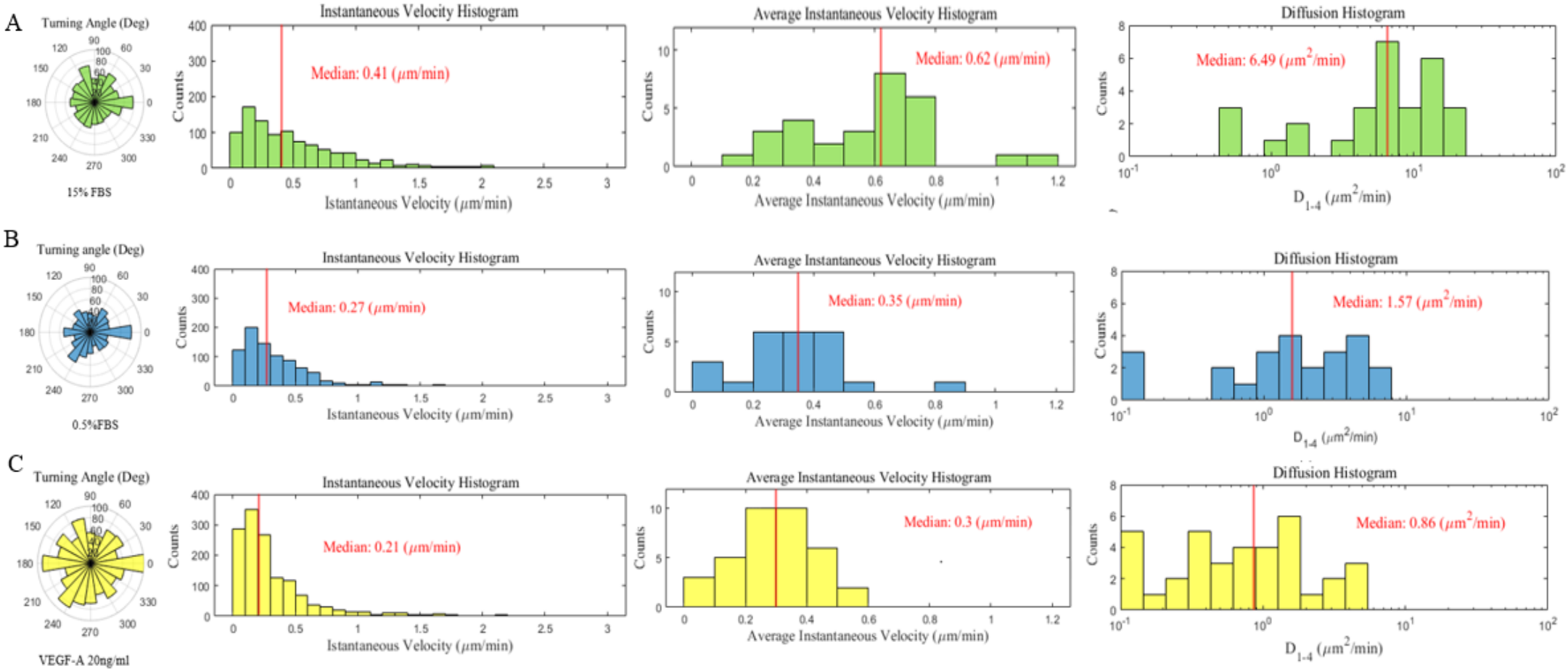

Figure 27. Cell Tracking Results. The Figure show the polar histogram, instantaneous velocity histogram, average instantaneous velocity histogram and the diffusion histogram of (A) cells with 15% FBS (green); (B) cells with 0.5% FBS (blue) and (C) cells under 20ng/ml of VEGF-A treatment. The median of each parameter is indicated in red.

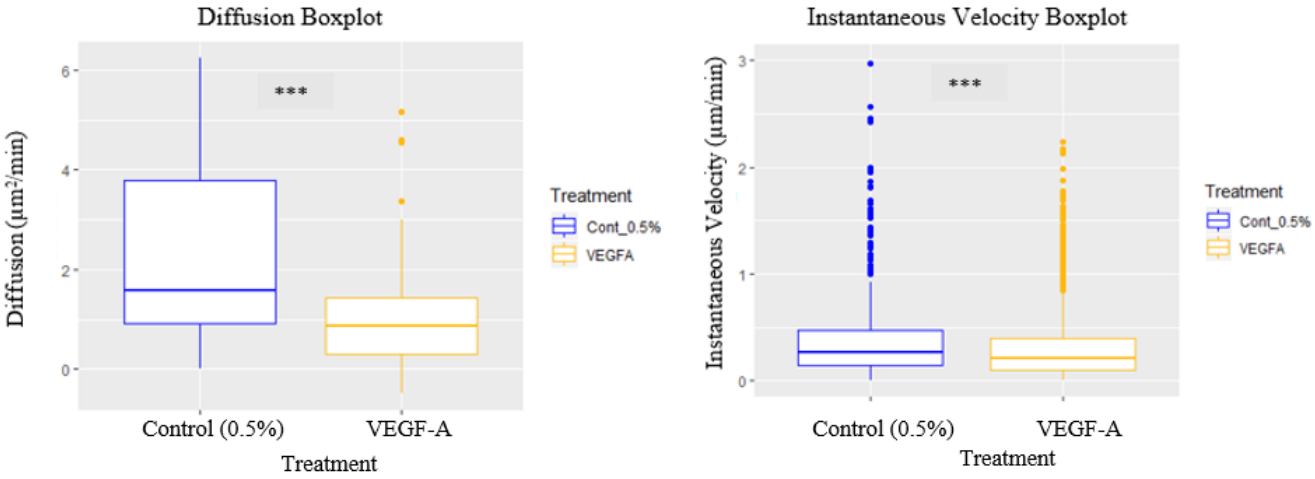

Figure 28. Cell tracking results represented as boxplot. The figure shows the diffusion values (left) and the instantaneous velocity of the cell tracking under VEGFA treatment (yellow) and control (blue respectively). Wilcoxon signed-rank test statistic test shows a significant difference. (***) indicates a $P \leq 0.001$.

4.4 Single Particle Tracking

4.4.1 VEGF-R1 Antibody selection for SPT experiments

We used the UCSF Chimera visualization Software to model VEGF-R1 along with VEGFA and a reduced immunoglobulin G. By marking in red the binding site of the antibody we could see if it will block the interaction between the receptor and its ligand.

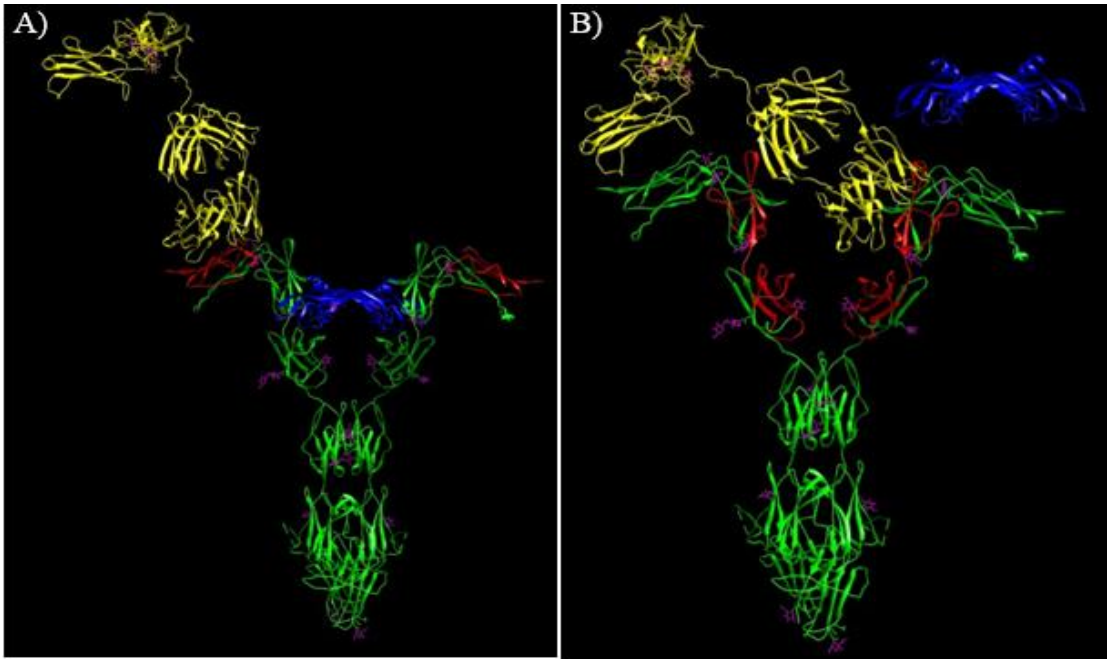

Figure 29. Ribbon drawing of crystallized VEGF-R1 and reduced IgG. VEGF-R1 (green); reduced Immunoglobulin G (yellow); VEGF-A (blue); glycosylations (Purple) and Antibody binding site (Red). (A)Represents antibody SY09-09/ MA5-32045 which does not block the binding site. (B) Represents antibody 720043 which blocks the VEGF-A binding site of VEGF-R1. Crystal structure from PDB: 5T89 (VEGF-R1 co-crystallized with VEGF-A) and partial structure of 1IGY (IgG).

4.4.2 Integrin $\alpha_5\beta_1$ Diffusion under VEGF-A treatment

Since integrin diffusion is a valuable proxy for identification of integrin conformation and its linkage to the actin cytoskeleton, we have used SPT to assess integrin $\alpha_5\beta_1$ diffusion under a 20ng/ml of VEGF-A treatment in human dermo fibroblasts.

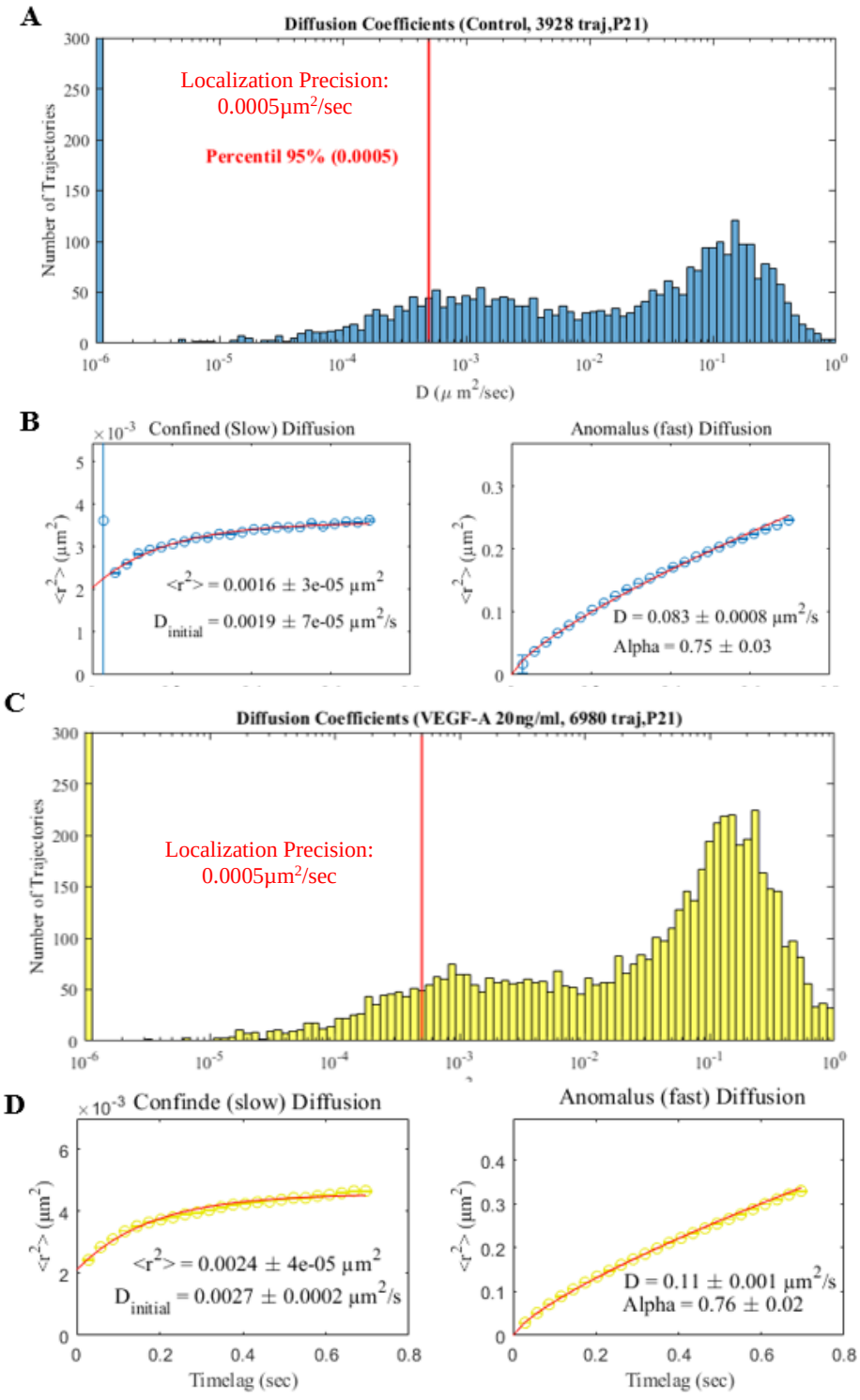

Figure 30. Integrin α5β1 Diffusion Analysis Results under VEGF-A treatment. (A and C) Histograms showing the diffusion coefficient of all the trajectories under VEGF-A treatment (Yellow) and control (Blue). P21 refers to the passage number. Red line shows the localization precision value. (B and D) Results of PDSD analysis under VEGF-A treatment (Yellow) and control (Blue). Right: confined trajectories (slow), r^2 shows the mean area of the confinement and $D_{initial}$ is the initial diffusion. Left: Anomalous trajectories (fast), Alpha is the exponential used for the fit.

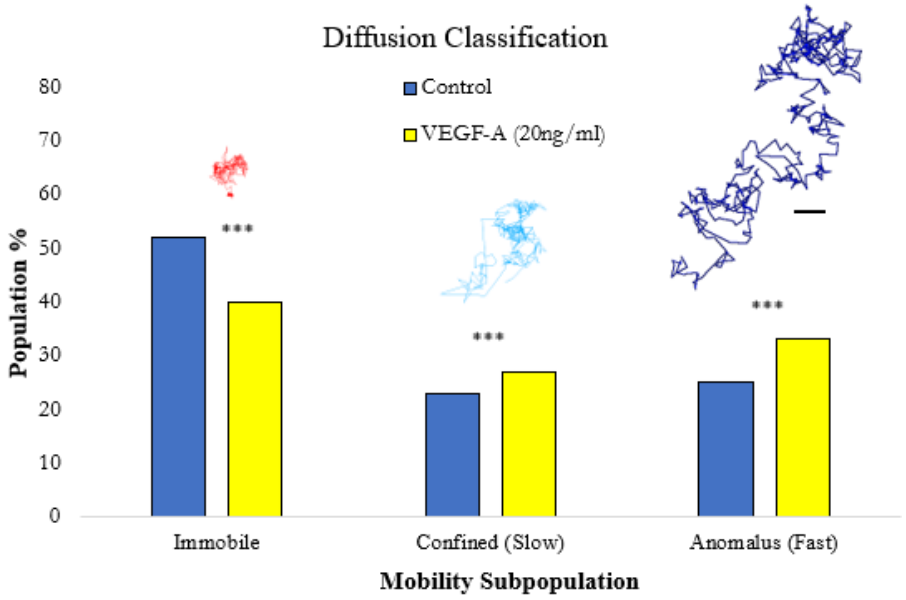

Figure 31. Integrin α5β1 Diffusion Trajectory Classification under VEGF-A treatment. Exemplary trajectories corresponding to different diffusion modalities (immobile, slow/confined and fast/free diffusion). The bar plot shows the percentage of occurrence of each diffusion classification observed under control and VEGF-A treatment. Pearson's chi-squared statistic test shows a significant difference. (***) indicates a $P \leq 0.001$. Scale bar 900nm

5. Discussion

5.1 Protein-Protein Interaction Data Bases: Integrin $\alpha_5\beta_1$and VEGF-R1

Due to previous reported interactions of integrins with different growth receptors [85] and given the importance of integrin $\alpha_5\beta_1$ and VEGF-A in the wound healing process we wanted to find out whether or not there was a described interaction between integrin $\alpha_5\beta_1$ and one of the VEGF-A receptors expressed by fibroblasts ,VEGF-R1.

At first, we relayed on PubMed to try to find any possible interaction. However, the amount of literature that contained our research keywords ($\alpha_5\beta_1$, VEGF-R1, interaction, direct, indirect) was very time consuming to examine so we decided to search in PPI databases where information about all interactions are derived from literature curation.

As you can see from figure 23 at the time, we did the PPI database exploration, $\alpha_5\beta_1$ directly interacts with uPAR (shown in light blue) through the β_1 subunit, uPAR and $\alpha_5\beta_1$ co-cluster upon VEGF-A treatment which leads to redistribution to focal adhesions at the leading edge of endothelial cells of both uPAR and $\alpha_5\beta_1$ [86]. In figure 23 we can also see how $\alpha_5\beta_1$ interacts with Tie2 (shown in purple) via Tie2's ligand, Ang1. Ang-1 fires signalling pathways through Tie2 and $\alpha_5\beta_1$ receptors that cross-talk when Tie2/$\alpha_5\beta_1$ interaction occurs inducing motility in endothelial cells [87], VEGF-A treatment upregulates Tie2 which enables a migratory response to Ang1 [88].

In addition to these findings, we also found out that $\alpha_5\beta_1$ and NRP1(shown in pink in figure 22), VEGFA co-receptor, interact with each other. NRP1 on endothelial promotes the internalization of active $\alpha_5\beta_1$ integrin. Once endocytosed, active $\alpha_5\beta_1$ is then recycled to the cell surface, thus favouring the formation of new adhesion sites [89]. Other molecules on the interaction network shown in figure 23 like PI3K and FAK imply integrins and VEGFRs share important signaling molecules [90], these molecules are involved in the signaling cascade of focal adhesion formation [91].

The only direct interaction between $\alpha_5\beta_1$ and VEGF-R1, was between $\alpha_5\beta_1$ and the soluble version of VEGF-R1 (sVEGF-R1). sVEGF-R1 is secreted by endothelial cells and becomes a matrix-associated protein that is able to interact with the $\alpha_5\beta_1$. However, The role of this variant has not yet been defined [92].

All these interactions have been assessed only on endothelial cells. However, other cells including fibroblasts express similar proteins like uPAR, Tie2 and NRP1 so to further understand the effects of VEGF-A on non-endothelial cells, these interactions should be reassessed on fibroblast. Nonetheless, these findings can still help us design future experiments.

5.2 Solid Barrier Wound Healing Assay

We wanted to use the solid-barrier method to produce uniform wounds that respected the fibronectin coating due to the importance of the ECM in the wound healing process. At first, to produce the wound we directly used barriers made out entirely of PDMS, a negative mould was designed also with PTC Creo Parametric and 3D printed (See Annex B, Section 9.5). This approach has been used by several other research groups [93], [94], yet, it did not work for us. For our experiments we use culture dishes with a seeding area of 20 nm diameter which means our PDMS barrier had to be smaller than that, the other research groups used bigger culture dishes and thus their PDMS barrier was much bigger and unlike ours, it did not float when we added the culture medium. If the PDMS barrier floats, the cells can migrate under and no wound will be produced, so we opted for 3D print directly the solid barrier to make it heavier, which we called "positive barriers".

We designed two types "positive" barriers, one that anchored itself by the bottom part of the culture dish (Figure 24 A) and another one that anchored itself by the top part of the culture dish (Figure 24 B), both produce rectangular wounds that mimic the ones produced by the micropipette tip in a conventional scratch assay, producing a 0,9-1mm wound [44]. After seeding the cells, we realised that the latter did not allowed for even distribution of the culture medium, so we settled on the barrier that attaches itself at the bottom which allows an easy cell seeding through the top slits and even medium distribution. As you can see from figure 25, where we can see a comparison between the wounds created using the scratch assay method (A and B) and the solid barrier (C and D), the scratch assay wounds have irregular borders and differ in size and shape between assays, as seen in the profile line graph which means they are not reproducible, hampering statistical analysis. In addition, we can see how the fibronectin coating with the scratch method is removed and left intact in other areas (baseline of the profile line graph very irregular -Figure 25 A) implying that changes in migration rates not only will be influenced by the conditions we want to assess (different growth factors or different *in vitro* ages) but also by the irregularities of the coating. Our barrier produced regular wounds and no significant damage to the fibronectin coating can be observed (baseline of the profile line is flat). We also designed other types of barriers like the ones shown in Figure 24 C which produces round-shape wounds, this wound morphology is more similar to chronic wound shapes and Figure 24 D shows a barrier that will produce a cross-shaped barrier.

We could not evaluate the wound closure rate between cells treated with VEGF-A and non-treated cells because we realised that many cells near the solid barrier were dead (rounded morphology) even though we tested the barrier biocompatibility before proceeding with the experiments (See Annex B: Section 9.2). We speculate that the cytotoxicity was due to the isopropyl used to cure the solid barrier, which seeped out through the PDMS pours. Under normal circumstances, we would have further evaluate the cytotoxicity of the barrier, try to find out other ways to cure the solid barrier, or to find a non-pours biocompatible polymer to replace the PDMS and repeated the wound healing assay experiments, but this was not possible due to the COVID-19 lockdown.

5.3 Cell Tracking

5.3.1 Cell Tracking Pipeline

For a normal wound healing assay, you only need to calculate the closure rate (collective migration). However, since we had images of migrating cells, we wanted to further exploit them to calculate the MSD, instantaneous velocity and turning angle of each cell as another way to evaluate the VEGF-A treatment. Due to the increasing popularity of cell tracking, nowadays there are several software that allows you to track cells. We decided to try two free open source software out: *Image J* manual tracking, due to its popularity and *Ilastik* which brings machine-learning-based bioimage analysis to end-users without substantial computational expertise [79]. We analysed the same images with *Image J*; *Ilastik* automatic tracking; *Ilastik* manual tracking and *Ilastik* manual tracking with an extra step that allowed us to manually check and revise each trajectory with *Matlab* (Explained in Section 3.2.4) (See ***Table 1*** for a summary).

When making our final decision about which software we were going to use we prioritised the trajectory length because we needed long trajectories to calculate the MSD, diffusion coefficient and instantaneous velocity. Furthermore, even though *Image J*, seems the most adequate due to its low consuming time and trajectory length, when tracking with *Image J* the users select manually the cell (coordinate) which can lead to errors. *Ilastik*, on the other hand, allows for image segmentation (See Figure 26 A), meaning, each cell is transformed into an object and the coordinates are extracted always from the centre of the object.

However, *Ilastik* faces the same challenges that every automatic cell tracking software has to deal with: cells which are not labelled with any fluorescent probe are similar to the background which makes it difficult for the algorithm to differentiate between them; there is a high variation in cell size and shape (this problem is accentuated with fibroblast which morphology changes are drastic while migrating) and some cells overlap with each other (See Figure 26 B, Cell 1 and 7) meaning it will start tracking one cell and eventually will start to track the neighbouring cell and treat the trajectory as if it was from only one cell [49]. So, to try to solve these obstacles, Dr. Carlo Manzo created a *Matlab* script to manually curate each cell track, so we made sure each track was from the same cell and filled in any missing coordinates to make long trajectories for the calculations. Thus, even though this option is the most time consuming it combines the advantages from both software, cell segmentation (accuracy) and trajectory length (needed for better analysis of the tracks).

5.3.2 Cell Tracking under VEGF-A treatment

Cells under 2D culture conditions, like our case, show random motility driven by multiple peripheral cell protrusions [95] this is what we can see in the polar histograms (Figure 27) of the three conditions (15% FBS, 0.5%FBS and VEGF-A), a behaviour that can be transformed into directed migration when there is a stimulus such as the cell-free area created by a wound. This can be seen in the polar histograms because there is a tendency of the motion vectors' distribution towards angle 0º, we consider that this is not as accentuated as we thought it would be at first due to the fact that there were no well-defined wounds due to cytotoxicity of the solid barrier used to produce them.

Fibroblasts cultured with 15% FBS (Figure 27 A) were used to set up the tracking pipeline and show a median instantaneous velocity of 0.41 µm/min which coincides with other published fibroblasts' velocities [93] and [94]. Furthermore, form the average instantaneous velocity graph we can distinguish two peaks, one around 0.3µm/min and the second one around 0.7µm/min which based on literature findings we think these peaks may correspond to areas of low and high cell density, areas with less cell density will allow cells to migrate faster than high cell density area [98] but this needs to be checked by examining if the tracks of said peaks correspond to low or high density areas but we did not have time. We could not find diffusion parameters of dermal fibroblasts in the literature to compare with ours, but it is a valuable measurement to calculate because it provides a measure of persistence, meaning how well the direction of migration is maintained [99].

As we can see from figure 28, there is a significant decrease in instantaneous velocity and diffusion in the VEGF-A treated fibroblasts (0.21µm/min and 0.86μm^2/min) compared to control fibroblasts (0.27µm/min and 1.57μm^2/min). So, despite 20ng/ml being enough to increase migration in endothelial cells [100] it was not enough to increase fibroblast migration. Emphasis should be made on the fact that the solid barrier assay was performed at PDL16 which corresponds to a high *in vitro* age, and VEGF-R1 expression is reduced with ageing [26]. Moreover, fibroblasts unlike endothelial cells, only express VEGF-R1. VEGF-R1 kinase activity is poor and does not stimulate downstream signalling cascades as efficiently as VEGF-R2 [101], this inadequate signal transduction and age-related receptor expression issues could explain the lack of stimulus by the VEGF-A treatment on fibroblast. In addition, an increase in fibroblast migration has been reported under 100ng/ml of VEGF-A but only on fibroblast from the edge of the wound, fibroblast migration was significantly reduced at the non-healing edge [74], our cell tracking was not performed on fibroblasts at the edge of the wound because due to cytotoxicity of the solid barrier there were no well-defined wounds. Although the cytotoxicity present in the samples may have affected how the cells have responded to the treatment, it was present in treated and control samples so, that makes us think that the changes that we see are due to the treatment. Nonetheless, these experiments will have to be repeated to confirm the results. Finally, to complement these findings, it is crucial to perform wound healing assays with fibroblasts at different PDLs, at higher concentrations than 20ng/ml and cell tracking should be performed at different

locations, this way we will be able to assess age-related, dose-related and zone-related effects of VEGF-A on fibroblasts.

5.4 Single-Particle Tracking

5.4.1 Antibody Selection

For SPT experiments it is crucial to select an adequate antibody because it is the way we label our protein of interest. For SPT experiments of VEGF-R1, we wanted an antibody that did not block the interaction site with VEGF-A so, after selecting extracellular antibodies we visualize, using the *UCSF Chimera* software, their binding site on VEGF-R1. As we can see from figure 29 A, antibody SY09-09 binds to D1 domain leaving the VEGF-A binding free. Due to Covid-19 lockdown, we did not get the chance to perform SPT experiments on VEGF-R1, but we were able to reduce it along with the 555651 antibody which targets the α_5 integrin subunit. As you can see in Annex A Section 9.1, on the SDS-PAGE gel we can see a band at around 75-88kDa which indicates that the antibody has been reduced between the disulphide bonds that hold on together the two heavy chains meaning the resulting antibody will only have one light-chain and one heavy chain and thus, it will only have one binding [64]. This will avoid artificial micro-clustering; this was demonstrated by previous results from the QuBiLab (not published). When using a reduced antibody, the proportion of confined diffusions were lower than when using a whole antibody indicating better integrin mobility through the cell membrane.

5.4.2 Integrin $\alpha_5\beta_1$ Diffusion under VEGF-A treatment

We performed single particle tracking studies to measure the diffusion of $\alpha_5\beta_1$ integrins, revealing a reduction in the percentage of immobile $\alpha_5\beta_1$ integrins under VEGF-A treatment, with a consequent increase in the slow and fast diffusion fractions (Figure 31). Furthermore, as you can see in figure 30 B and D, the initial diffusion of both (confined and anomalous) under the VEGF-A treatment (0.0024μm^2/sec and 0.11 μm^2/sec, respectively) are higher than the initial diffusion of the control sample (0.0019μm^2/sec and 0.083 μm^2/sec, respectively). Additionally, the radius of confinement ($<r^2>$) was larger in the treated samples (0.0024 μm^2) than in the control (0.0016 μm^2). This indicates that not only there is an increase in mobile integrin but also that they move faster through the cell membrane.

This decrease in immobile $\alpha_5\beta_1$ integrins means that less $\alpha_5\beta_1$ integrins are interacting with their ligand (fibronectin). If there are fewer integrins anchored to their ligand it means that the cells generate fewer traction forces and could be translated to a decrease in migration. Another explanation for a reduction in immobile $\alpha_5\beta_1$ could be explained by an increase in integrin trafficking as we have seen that happens with the indirect interactions uPAR and Tie2 under VEGF-A treatment (See Section 5.1) but this cannot be assessed by SPT experiments.

These results cannot be compared with the tracking results because there was no cytotoxic substances present in the diffusion experiments. Moreover, these experiments were carried out at different PDLs (different *in vitro* ageing) and from other QuBiLab experiments we know that integrin $\alpha_5\beta_1$ diffusion changes with different *in vitro* ages.

6. Conclusions

We have managed to create a solid barrier that creates uniform wounds and respects the fibronectin coating maintaining the simplicity and low-cost characteristics of the conventional method (scratch assay). However, before using it again its cytotoxicity should be evaluated to avoid putting at risk future experiments.

By combining the advantages of two cell tracking software we have been able to create a cell tracking pipeline that will enable us to extract more data form the wound healing assay images and thus, complement our research with further statistical analysis.

From the bibliographical and protein-protein interaction database search we have reached to the conclusion that there is a three-way relationship between integrin $\alpha_5\beta_{1,}$ VEGF-A and VEGF-R1 which is more indirect than direct. Nonetheless, there are some evidence of a direct interaction of integrin $\alpha_5\beta_1$ with the soluble isoform of VEGF-R1. Emphasis should be made that even though fibroblasts express the same proteins that have been reported to interact with integrin $\alpha_5\beta_1$ these findings have only been done in endothelial cells.

Despite the fact that the solid barrier was toxic and proper wound healing assays could not be performed; our cell tracking results make us believe that VEGF-A has a negative effect on fibroblasts. However, to fully assess and understand this effect one should consider the dose of VEGF-A administered to the cells, the *in vitro* age of the cells and the area (wound healing edge/ non-wound healing edge). We had these considerations in mind and planned on doing these experiments, but we were not able to perform them due to the COVID-19 lockdown. Nonetheless, the few experiments we performed reinforce the need of taking into account the variables mentioned above.

The effect of VEGF-A on fibroblast was not only evaluated at a cellular level but also to molecular level by performing single particle tracking studies to measure the diffusion of $\alpha_5\beta_1$, revealing a reduction in the percentage of immobile $\alpha_5\beta_1$. In the future, we plan to perform the same single particle tracking experiments with different concentrations of VEGF-A and different *in vitro* ages and also perform SPT assays on VEGF-R1.

All in all, we believe that more in-depth work should be done to shed a light on the broader role that, clearly, VEGF-A plays in the wound healing process, especially in non-endothelial cells such as fibroblasts.

7. Bibliography

[1] F. Gottrup, 'A specialized wound-healing center concept: Importance of a multidisciplinary department structure and surgical treatment facilities in the treatment of chronic wounds', *Am. J. Surg.*, vol. 187, no. 5 SUPPL. 1, pp. S38–S43, May 2004.

[2] K. E. Johnson and T. A. Wilgus, 'Vascular Endothelial Growth Factor and Angiogenesis in the Regulation of Cutaneous Wound Repair', *Adv. Wound Care*, vol. 3, no. 10, pp. 647–661, Oct. 2014.

[3] K. W. Ng. and W. M. Lau., 'Skin Deep: The Basics of Human Skin Structure and Drug Penetration', *Percutaneous Penetration Enhanc. Chem. Methods Penetration Enhanc. Drug Manip. Strateg. Veh. Eff.*, no. January, pp. 1–341, 2015.

[4] W. D. James, T. G. Berger, and D. M. Elston, *Diseases of the Skin*, vol. 21, no. 1. 1980.

[5] K. A. Bielefeld, S. Amini-Nik, and B. A. Alman, 'Cutaneous wound healing: Recruiting developmental pathways for regeneration', *Cell. Mol. Life Sci.*, vol. 70, no. 12, pp. 2059–2081, 2013.

[6] H. E. DesJardins-Park, S. Mascharak, M. S. Chinta, D. C. Wan, and M. T. Longaker, 'The spectrum of scarring in craniofacial wound repair', *Front. Physiol.*, vol. 10, no. MAR, Mar. 2019.

[7] M. Rodrigues, N. Kosaric, C. A. Bonham, and G. C. Gurtner, 'Wound healing: A cellular perspective', *Physiol. Rev.*, vol. 99, no. 1, pp. 665–706, Jan. 2019.

[8] A. J. Singer and R. A. F. Clark, 'Cutaneous wound healing', *New England Journal of Medicine*, vol. 341, no. 10. pp. 738–746, 02-Sep-1999.

[9] WoundSource Editors, 'The Four Stages of Wound Healing | Wound Source'. [Online]. Available: https://www.woundsource.com/blog/four-stages-wound-healing. [Accessed: 18-Mar-2020].

[10] W. A. Robert, *The Biology of Cancer*, Second. Garland Science.

[11] Gregory S. Schultz, Glenn Ladwig., and Annette Wysocki, 'Extracellular matrix: review of its roles in acute and chronic wounds', Aug-2005. [Online]. Available: http://www.worldwidewounds.com/2005/august/Schultz/Extrace-Matric-Acute-Chronic-Wounds.html#extracellular-matrix. [Accessed: 16-Mar-2020].

[12] C. Frantz, K. M. Stewart, and V. M. Weaver, 'The extracellular matrix at a glance', *J. Cell Sci.*, vol. 123, no. 24, pp. 4195–4200, 2010.

[13] J. K. Kular, S. Basu, and R. I. Sharma, 'The extracellular matrix: Structure, composition, age-related differences, tools for analysis and applications for tissue engineering', *J. Tissue Eng.*, vol. 5, 2014.

[14] C. D. Paul, W.-C. Hung, D. Wirtz, and K. Konstantopoulos, 'Engineered Models of Confined Cell Migration', *Annu. Rev. Biomed. Eng.*, vol. 18, no. 1, pp. 159–180, Jul. 2016.

[15] M. D. Lynch and F. M. Watt, 'Fibroblast heterogeneity: implications for human disease', *Journal of Clinical Investigation*, vol. 128, no. 1. American Society for Clinical Investigation, pp. 26–35, 02-Jan-2018.

[16] T. H. Chun and M. Inoue, '3-D adipocyte differentiation and peri-adipocyte collagen turnover', in *Methods in Enzymology*, vol. 538, Academic Press Inc., 2014, pp. 15–34.

[17] S. Rhee, 'Fibroblasts in three dimensional matrices: Cell migration and matrix remodeling', *Experimental and Molecular Medicine*, vol. 41, no. 12. Nature Publishing Group, pp. 858–865, 31-Dec-2009.

[18] M. L. De Ieso and A. J. Yool, 'Mechanisms of aquaporin-facilitated cancer invasion and metastasis', *Front. Chem.*, vol. 6, 2018.

[19] M. Nistal, P. Sesma, M. Álvarez-Uría, B. Fraile, R. Anadón, and F. J. Sáez, *Biologi-a celular*. .
[20] G. Jacquemet, H. Hamidi, and J. Ivaska, 'Filopodia in cell adhesion, 3D migration and cancer cell invasion', *Current Opinion in Cell Biology*, vol. 36. Elsevier Ltd, pp. 23–31, 01-Oct-2015.
[21] S. Kroening and M. Goppelt-Struebe, 'Analysis of matrix-dependent cell migration with a barrier migration assay', *Sci. Signal.*, vol. 3, no. 126, pp. 1–11, 2010.
[22] C. De Pascalis and S. Etienne-Manneville, 'Single and collective cell migration: The mechanics of adhesions', *Molecular Biology of the Cell*, vol. 28, no. 14. American Society for Cell Biology, pp. 1833–1846, 07-Jul-2017.
[23] P. Friedl and K. Wolf, 'Proteolytic interstitial cell migration: A five-step process', *Cancer and Metastasis Reviews*, vol. 28, no. 1–2. Springer Netherlands, pp. 129–135, 2009.
[24] S. Qin, R. A. F. Clark, and M. H. Rafailovich, 'Establishing correlations in the en-mass migration of dermal fibroblasts on oriented fibrillar scaffolds', *Acta Biomater.*, vol. 25, pp. 230–239, Oct. 2015.
[25] E. Scarpa and R. Mayor, 'Collective cell migration in development', *J. Cell Biol.*, vol. 212, no. 2, pp. 143–155, Jan. 2016.
[26] A. Berthaut *et al.*, 'Vascular endothelial growth factor receptor-1 (VEGFR-1) expression in human corneal fibroblast decreased with age', 2009.
[27] K. J. Pienta and D. S. Coffey, 'Characterization of the subtypes of cell motility in ageing human skin fibroblasts', *Mech. Ageing Dev.*, vol. 56, no. 2, pp. 99–105, Nov. 1990.
[28] S. Sethe, A. Scutt, and A. Stolzing, 'Aging of mesenchymal stem cells', *Ageing Research Reviews*, vol. 5, no. 1. Elsevier Ireland Ltd, pp. 91–116, Feb-2006.
[29] S. Geißler *et al.*, 'Functional Comparison of Chronological and In Vitro Aging: Differential Role of the Cytoskeleton and Mitochondria in Mesenchymal Stromal Cells', *PLoS One*, vol. 7, no. 12, Dec. 2012.
[30] T. Ahsan, 'Best Practices in MSC Culture: Tracking and Reporting Cellular Age Using Population Doubling Level (PDL) and not Passage Number - RoosterBio'. [Online]. Available: https://www.roosterbio.com/mscs-characterization/best-practices-in-msc-culture-tracking-and-reporting-cellular-age-using-population-doubling-level-pdl-and-not-passage-number/. [Accessed: 22-Mar-2020].
[31] T. Tadokoro *et al.*, 'Preferential reduction of the α-2-6-sialylation from cell surface N-glycans of human diploid fibroblastic cells by in vitro aging', *Glycoconj. J.*, vol. 23, no. 5–6, pp. 443–452, Jul. 2006.
[32] Y. Itakura, N. Sasaki, D. Kami, S. Gojo, A. Umezawa, and M. Toyoda, 'N - and O - glycan cell surface protein modifications associated with cellular senescence and human aging', *Cell Biosci.*, pp. 1–11, 2016.
[33] P. P. Ongusaha *et al.*, 'HB-EGF is a potent inducer of tumor growth and angiogenesis', *Cancer Res.*, vol. 64, no. 15, pp. 5283–5290, Aug. 2004.
[34] K. Kawada *et al.*, 'Cell Migration Is Regulated by Platelet-Derived Growth Factor Receptor Endocytosis', *Mol. Cell. Biol.*, vol. 29, no. 16, pp. 4508–4518, Aug. 2009.
[35] H. Shi *et al.*, 'bFGF promotes the migration of human dermal fibroblasts under diabetic conditions through reactive oxygen species production via the PI3K/Akt-Rac1- JNK pathways', *Int. J. Biol. Sci.*, vol. 11, no. 7, pp. 845–859, Jun. 2015.
[36] A. Berthaut *et al.*, 'Insulin growth factor promotes human corneal fibroblast network formation in vitro', *Investig. Ophthalmol. Vis. Sci.*, vol. 52, no. 10, pp. 7647–7653, Sep. 2011.

[37] S. Werner and R. Grose, ‘Regulation of Wound Healing by Growth Factors and Cytokines’, 2003.
[38] A. T. Grazul-Bilska *et al.*, ‘Wound healing: The role of growth factors’, *Drugs of Today*, vol. 39, no. 10, pp. 787–800, 2003.
[39] H. Ejiri *et al.*, ‘Use of synthetic serum-free medium for culture of human dermal fibroblasts to establish an experimental system similar to living dermis’, *Cytotechnology*, vol. 67, no. 3, pp. 507–514, May 2015.
[40] A. Ozcelikkale, J. C. Dutton, F. Grinnell, and B. Han, ‘Effects of dynamic matrix remodelling on en masse migration of fibroblasts on collagen matrices’, *J. R. Soc. Interface*, vol. 14, no. 135, Oct. 2017.
[41] J.-Y. Lin, K.-Y. Lo, and Y.-S. Sun, ‘Effects of Substrate-Coating Materials on the Wound-Healing Process’, 2019.
[42] D. Missirlis, T. Haraszti, H. Kessler, and J. P. Spatz, ‘Fibronectin promotes directional persistence in fibroblast migration through interactions with both its cell-binding and heparin-binding domains’, *Sci. Rep.*, vol. 7, no. 1, pp. 1–16, Dec. 2017.
[43] W. Li *et al.*, ‘Mechanism of Human Dermal Fibroblast Migration Driven by Type I Collagen and Platelet-derived Growth Factor-BB’, *Mol. Biol. Cell*, vol. 15, pp. 294–309, 2004.
[44] W. J. Ashby and A. Zijlstra, ‘Established and novel methods of interrogating two-dimensional cell migration’, *Integrative Biology (United Kingdom)*, vol. 4, no. 11. NIH Public Access, pp. 1338–1350, 2012.
[45] IIBm, Universidad Autonoma de Madrid, CSIC, and Ministro de Ciencia e Innovación, ‘Protocolo de ensayo de herida’, pp. 1–14, 2013.
[46] S. R. K. Vedula, A. Ravasio, C. T. Lim, and B. Ladou, ‘Collective cell migration: A mechanistic perspective’, *Physiology*, vol. 28, no. 6. pp. 370–379, 01-Nov-2013.
[47] J. E. N. Jonkman *et al.*, ‘An introduction to the wound healing assay using live-cell microscopy’, vol. 8, no. 5, pp. 440–451, 2014.
[48] A. Stamm, K. Reimers, S. Strauß, P. Vogt, T. Scheper, and I. Pepelanova, ‘In vitro wound healing assays - State of the art’, *BioNanoMaterials*, vol. 17, no. 1–2. Walter de Gruyter GmbH, pp. 79–87, 01-May-2016.
[49] E. Meijering, O. Dzyubachyk, and I. Smal, ‘Methods for Cell and Particle Tracking’, Elsevier, 2012.
[50] X. Michalet, ‘Mean Square Displacement Analysis of Single-Particle Trajectories with Localization Error: Brownian Motion in Isotropic Medium’.
[51] A. Triller and D. Choquet, ‘New Concepts in Synaptic Biology Derived from Single-Molecule Imaging’, *Neuron*, vol. 59, no. 3. Elsevier, pp. 359–374, 14-Aug-2008.
[52] P. Bainbridge, ‘Wound healing and the role of fibroblasts’, *J. Wound Care*, vol. 22, no. 8, pp. 407–412, 2013.
[53] J. Schnittert, R. Bansal, G. Storm, and J. Prakash, ‘Integrins in wound healing, fibrosis and tumor stroma: High potential targets for therapeutics and drug delivery’, *Adv. Drug Deliv. Rev.*, vol. 129, pp. 37–53, 2018.
[54] ‘Integrin Biology – Morphic Therapeutic’. [Online]. Available: https://morphictx.com/our-technology/. [Accessed: 21-Mar-2020].
[55] J. Ivaska and J. Heino, ‘Cooperation Between Integrins and Growth Factor Receptors in Signaling and Endocytosis’, *Annu. Rev. Cell Dev. Biol.*, vol. 27, no. 1, pp. 291–320, 2011.
[56] Y. Su *et al.*, ‘Relating conformation to function in integrin α 5 β 1’.
[57] N. Nishida, C. Xie, M. Shimaoka, Y. Cheng, T. Walz, and T. A. Springer,

‘Activation of Leukocyte β2 Integrins by Conversion from Bent to Extended Conformations’, *Immunity*, vol. 25, no. 4, pp. 583–594, Oct. 2006.
[58] B. Geiger and K. M. Yamada, ‘Molecular architecture and function of matrix adhesions’, *Cold Spring Harb. Perspect. Biol.*, vol. 3, no. 5, pp. 1–21, 2011.
[59] L. Koivisto, J. Heino, L. Häkkinen, and H. Larjava, ‘Integrins in Wound Healing’, *Adv. Wound Care*, vol. 3, no. 12, pp. 762–783, 2014.
[60] M. E. Janik, A. Lityńska, and P. Vereecken, ‘Cell migration-The role of integrin glycosylation’, *Biochimica et Biophysica Acta - General Subjects*, vol. 1800, no. 6. pp. 545–555, Jun-2010.
[61] C. Manzo and M. F. Garcia-Parajo, ‘A review of progress in single particle tracking: from methods to biophysical insights’, *Reports Prog. Phys.*, vol. 78, no. 12, p. 124601, Oct. 2015.
[62] S. Anthony, L. Zhang, and S. Granick, ‘Methods to track single-molecule trajectories’, *Langmuir*, vol. 22, no. 12, pp. 5266–5272, Jun. 2006.
[63] F. Pinaud, S. Clarke, A. Sittner, and M. Dahan, ‘Probing cellular events, one quantum dot at a time’, *Nature Methods*, vol. 7, no. 4. pp. 275–285, 30-Apr-2010.
[64] D. T. Clarke and M. L. Martin-Fernandez, ‘A Brief History of Single-Particle Tracking of the Epidermal Growth Factor Receptor’, *Methods Protoc.*, vol. 2, no. 1, p. 12, 2019.
[65] ‘Antibody Structure - Bio X Cell’. [Online]. Available: https://bxcell.com/antibody-structure/. [Accessed: 08-Mar-2020].
[66] ‘Qdot Nanocrystals—Section 6.6 | Thermo Fisher Scientific - ES’. [Online]. Available: https://www.thermofisher.com/es/es/home/references/molecular-probes-the-handbook/ultrasensitive-detection-technology/qdot-nanocrystal-technology.html. [Accessed: 08-Mar-2020].
[67] D. S. Lidke *et al.*, ‘Exploring membrane protein dynamics by multicolor single quantum dot imaging using wide field, TIRF, and hyperspectral microscopy’, in *Colloidal Quantum Dots for Biomedical Applications II*, 2007, vol. 6448, p. 64480Y.
[68] Y. Yang, T. Xia, W. Zhang, and X. H. Fang, ‘Single-molecule fluorescence imaging of membrane-bound proteins for studies of cell signal transduction’, *Chinese Science Bulletin*, vol. 56, no. 11. pp. 1063–1067, 26-Apr-2011.
[69] G. J. Schuitz, H. Schindler, and T. Schmidt, ‘Single-Molecule Microscopy on Model Membranes Reveals Anomalous Diffusion’, 1997.
[70] ‘Informe de la Agencia Española de Medicamentos y Productos Sanitarios sobre el uso de Plasma Rico en Plaquetas’.
[71] K. M. Lacci and A. Dardik, ‘Platelet-rich plasma: Support for its use in wound healing’, *Yale Journal of Biology and Medicine*, vol. 83, no. 1. Yale Journal of Biology and Medicine, pp. 1–9, Mar-2010.
[72] B. L. Eppley, J. E. Woodell, and J. Higgins, ‘Platelet quantification and growth factor analysis from platelet-rich plasma: Implications for wound healing’, *Plast. Reconstr. Surg.*, vol. 114, no. 6, pp. 1502–1508, 2004.
[73] Y. Cao, ‘Positive and negative modulation of angiogenesis by VEGFR1 ligands’, *Science Signaling*, vol. 2, no. 59. pp. re1–re1, 24-Feb-2009.
[74] H. Brem *et al.*, ‘Mechanism of Sustained Release of Vascular Endothelial Growth Factor in Accelerating Experimental Diabetic Healing’, *J. Invest. Dermatol.*, vol. 129, pp. 2275–2287, 2009.
[75] T. A. Wilgus *et al.*, ‘Novel function for vascular endothelial growth factor receptor-1 on epidermal keratinocytes’, *Am. J. Pathol.*, vol. 167, no. 5, pp. 1257–1266, 2005.

[76] A. Berthaut *et al.*, 'Vascular endothelial growth factor receptor-1 (VEGFR-1) expression in human corneal fibroblast decreased with age', *Mol. Vis.*, vol. 15, no. September, pp. 1997–2007, 2009.
[77] F. Cianfarani *et al.*, 'Placenta growth factor in diabetic wound healing: Altered expression and therapeutic potential', *Am. J. Pathol.*, vol. 169, no. 4, pp. 1167–1182, 2006.
[78] V. Casquillas and T. Houssin, 'PDMS: A Review', *Elveflow*, 2015.
[79] S. Berg *et al.*, 'ilastik: interactive machine learning for (bio)image analysis', *Nat. Methods*, vol. 16, no. 12, pp. 1226–1232, Dec. 2019.
[80] 'DTT 1,4-Dithiothreitol, Sigma-Aldrich'. [Online]. Available: https://www.sigmaaldrich.com/catalog/product/roche/dttro?lang=es&region=ES. [Accessed: 08-Mar-2020].
[81] 'Iodoacetamide BioUltra, Sigma-Aldrich'. [Online]. Available: https://www.sigmaaldrich.com/catalog/product/sigma/i1149?lang=es&region=ES. [Accessed: 08-Mar-2020].
[82] Thermo Scientific, 'EZ-Link Sulfo-NHS-LC-Biotin A39257 21335'.
[83] J.-Y. Tinevez *et al.*, 'TrackMate: An open and extensible platform for single-particle tracking.', *Methods*, vol. 115, pp. 80–90, 2017.
[84] A. Sosa-Costa *et al.*, 'Lateral Mobility and Nanoscale Spatial Arrangement of Chemokine-activated α4β1 Integrins on T Cells', 2016.
[85] P. R. Somanath, A. Ciocea, and T. V. Byzova, 'Integrin and growth factor receptor alliance in angiogenesis', *Cell Biochem. Biophys.*, vol. 53, no. 2, pp. 53–64, Mar. 2009.
[86] J. M. Breuss and P. Uhrin, 'Cell Adhesion & Migration VEGF-initiated angiogenesis and the uPA/uPAR system', 2012.
[87] I. Cascone, L. Napione, F. Maniero, G. Serini, and F. Bussolino, 'Stable interaction between α5β1 integrin and Tie2 tyrosine kinase receptor regulates endothelial cell response to Ang-1', *J. Cell Biol.*, vol. 170, no. 6, pp. 993–1004, Sep. 2005.
[88] L. J. Metheny-Barlow, S. Tian, A. J. Hayes, and L. Y. Li, 'Direct chemotactic action of angiopoietin-1 on mesenchymal cells in the presence of VEGF', *Microvasc. Res.*, vol. 68, no. 3, pp. 221–230, Nov. 2004.
[89] D. Valdembri *et al.*, 'Neuropilin-1/GIPC1 signaling regulates α5β1 integrin traffic and function in endothelial cells', *PLoS Biol.*, vol. 7, no. 1, 2009.
[90] E. S. Wijelath *et al.*, 'Heparin-II domain of fibronectin is a vascular endothelial growth factor-binding domain: Enhancement of VEGF biological activity by a singular growth factor/matrix protein synergism', *Circ. Res.*, vol. 99, no. 8, pp. 853–860, Oct. 2006.
[91] 'KEGG PATHWAY: Focal adhesion - Homo sapiens (human)'. [Online]. Available: https://www.genome.jp/kegg-bin/show_pathway?select_scale=1.0&query=&map=hsa04510&scale=&image=%2Fshare%2Fwww%2F%2Fmark_pathway159076947543665%2Fhsa04510.png&orgs=&auto_image=&nocolor=&show_description=hide&multi_query=&module=. [Accessed: 30-May-2020].
[92] A. Orecchia, P. M. Lacal, C. Schietroma, V. Morea, G. Zambruno, and C. M. Failla, 'Vascular endothelial growth factor receptor-1 is deposited in the extracellular matrix by endothelial cells and is a ligand for the α5β1 integrin', *J. Cell Sci.*, vol. 116, no. 17, pp. 3479–3489, 2003.
[93] Y. Shiode *et al.*, 'A novel cell exclusion zone assay with a barrier made from room temperature vulcanizing silicone rubber', *PLoS One*, vol. 12, no. 12, pp. 1–12, 2017.

[94] D. M. Sherry, E. E. Parks, E. C. Bullen, D. L. Updike, and E. W. Howard, ‘A simple method for using silicone elastomer masks for quantitative analysis of cell migration without cellular damage or substrate disruption’, *Cell Adhes. Migr.*, vol. 7, no. 6, pp. 479–485, 2013.
[95] G. G. Reig, E. Pulgar, and M. L. Concha, ‘Cell migration: from tissue culture to embryos’, 2014.
[96] J. Kim, J. C. Park, M. H. Lee, C. E. Yang, J. H. Lee, and W. J. Lee, ‘High-mobility group box 1 mediates fibroblast activity via RAGE-MAPK and NF-κB signaling in keloid scar formation’, *Int. J. Mol. Sci.*, vol. 19, no. 1, p. 76, Jan. 2018.
[97] X. Trepat, Z. Chen, and K. Jacobson, ‘Cell Migration Single-Cell Migration’, *Compr. Physiol.*, pp. 2369–2392, Oct. 2012.
[98] M. Chun Leong, V. Sri Ram Krishna, C. Teck Lim, and B. Ladoux, ‘Geometrical constraints and physical crowding direct collective migration of fibroblasts’, 2013.
[99] C. P. McCann, P. W. Kriebel, C. A. Parent, and W. Losert, ‘Cell speed, persistence and information transmission during signal relay and collective migration’, *J. Cell Sci.*, vol. 123, no. 10, pp. 1724–1731, 2010.
[100] T. V Byzova *et al.*, ‘A Mechanism for Modulation of Cellular Responses to VEGF: Activation of the Integrins’, 2000.
[101] S. Koch and L. Claesson-Welsh, ‘Signal transduction by vascular endothelial growth factor receptors’, *Cold Spring Harbor Perspectives in Medicine*, vol. 2, no. 7. Cold Spring Harbor Laboratory Press, 2012.
[102] S. Werner and R. Grose, ‘Regulation of wound healing by growth factors and cytokines’, *Physiological Reviews*, vol. 83, no. 3. American Physiological Society, pp. 835–870, 2003.

8. Annex A: Summary Tables

Table 2 Summary of main Extracellular matrix components of the skin. The table shows their function and what happens to them during ageing and the wound healing process. Table made from information gathered from [11], [12], [59] .

Component	Function	Wound	Age
Collagen	Collagen in the dermal matrix is composed primarily of type I and III. Gives tensile strength to skin	Fibroblasts begin to synthesize and deposit large quantities of collagen type I and III	Collagen fibres are inappropriately crosslinked through glycation
Fibronectin	Glycoprotein with multiple functions due to many binding sites	Fibroblasts begin to synthesize and deposit large quantities of Fibronectin	Senescent fibroblasts typically express elevated levels of FN
Elastin	Elastin is composed of soluble tropoelastin. Tropoelastin when cross-linked forms an insoluble complex. It gives skin the required resilience to recoil after stretching.	Elastin fragments are generated during wound healing. These fragments are released into the ECM through protease action and can induce biological responses in cells through their role as biologically active ligands.	Elastin network integrity is destroyed by the elevated presence of metalloproteases
Laminin	A large protein made up of three polypeptide chains. contains specialised regions that bind to ECM proteins and Integrins.	Laminis are critical players in re-epithelialization and angiogenesis.	Reduced levels of Laminin compromise the integrity of the ECM. Elevated metalloproteases levels degrade Laminin
Glycosaminoglycans (GAGs)/ Proteoglycans (PGs)	PGs are composed of GAGs, which are polysaccharide chains made up of repeating disaccharide units which are strongly hydrophilic. This enables the ECM to withstand compression forces.	Promote transition of normal dermal fibroblasts to myofibroblasts and regulates wound healing through induction of angiogenesis	Reduced levels of tissue-associated GAGs compromise the integrity of the ECM.

Table 3 Summary of main Growth Factors. These growth factors are involved in wound healing, the table shows the cells they are released by and their main function. Table made from information gathered from:[102] and [38].

Growth Factor	Cell Source	Target Cell →Main Function
PDGF	Platelets. Macrophages. Monocytes. Fibroblasts. Endothelial cells	Fibroblasts → proliferation and ECM production. Neutrophils → chemoattractant. Monocytes →chemoattractant.
TGF-β	Platelets Macrophages, Lymphocytes, Fibroblasts, Keratinocytes	Fibroblasts → proliferation and ECM production and integrin expression. Neutrophils → chemoattractant. Monocytes →chemoattractant and growth factor secretion.
TGF-α	Platelets. Macrophages. Keratinocytes.	Epithelial → migration. Fibroblasts→migration.
EGF	Platelets Macrophages Fibroblasts Endothelial cells	Fibroblasts→migration and fibronectin production. Endothelial cells→migration. Keratinocytes→migration.
FGF	Fibroblasts. Macrophages. Endothelial cells. Keratinocytes.	Fibroblasts →mitogen and ECM synthesis. Endothelial cells →mitogen. Epithelial cells→mitogen. Keratinocytes →mitogen.
KGF	Fibroblasts.	Keratinocytes→proliferation, migration and morphogenesis.
VEGF	Platelets Macrophages. Fibroblasts. Keratinocytes.	Endothelial cells → migration and angiogenesis.
IGF	Macrophages Neutrophils Fibroblasts	Fibroblasts→ migration and proliferation. Epithelial cells→migration and migration.

Epidermal growth factor (EGF), fibroblast growth factor (FGF), insulin-like growth factor (IGF), keratinocyte growth factor (KGF), platelet-derived growth factor (PDGF), trans- forming growth factor (TGF) and vascular endothelial growth factor (VEGF).

Table 4 Summary of main antibodies against VEGF-R1. These antibodies were taken into account for possible candidates for SPT experiments.

Name (Product Number)	Manufacture	Used for	Host	Binding site	Clonality
VEGF Receptor 1 Antibody /PA5-32408	Invitrogen	ICC, IF, WB, IHC, IM	Rabbit	C-terminus (Intracellular)	Polyclonal
VEGF Receptor 1 Antibody/720043	Invitrogen	ICC, IF, WB	Rabbit	178-300aa (VEGF-A binding site)	Polyclonal
VEGF Receptor 1 Antibody/ PA5-16493	Invitrogen	WB ICC, ICH	Rabbit	C-terminus (Intracellular)	Polyclonal
VEGF Receptor 1 Antibody (SY09-09) /MA5-32045	Invitrogen	Flow, ICC, IF, IHC, WB	Rabbit	1-100 aa (Extracellular)	Monoclonal
VEGF Receptor 1 Antibody /PA1-21731	Invitrogen	IHC	Rabbit	1312-1328 aa (Intracellular)	Polyclonal
FLT1 Antibody, /H00002321-D01P	Abnova	WB	Rabbit	1-687aa (Extracellular)	Polyclonal
VEGF Receptor 1 Antibody (3D10)/ MA5-15550	Invitrogen	WB	Mouse	Extracellular fragment of human FLT1	Monoclonal
Phospho-VEGF Receptor 1 Antibody/ PA5-64564	Invitrogen	WB	Rabbit	Tyr1242 (Intracellular)	Polyclonal
Phospho-VEGF Receptor 1 Antibody	Invitrogen	IHC	Rabbit	Tyr1048 (Intracellular)	Polyclonal
Phospho-VEGF Receptor 1 Antibody	Invitrogen	WB	Rabbit	Tyr1333 (Intracellular)	Polyclonal
FLT1 Antibody/ H00002321-B01P	Abnova	WB, IF	Mouse	1- 687aa (Extracellular)	Polyclonal
FLT1 Monoclonal Antibody (OTI11G5)/ CF806786	OriGene	WB	Mouse	781-1338 aa (Intracellular)	Monoclonal

Western Blot (WB), Immunocytochemistry (ICC), Immunohistochemistry (IHC), Immunomicroscopy (IM), Flow Cytometry (Flow), Immunofluorescence (IF), amino acid (aa).

9. Annex B: Intermediate Results

9.1 Half Antibody SDS-PAGE gels

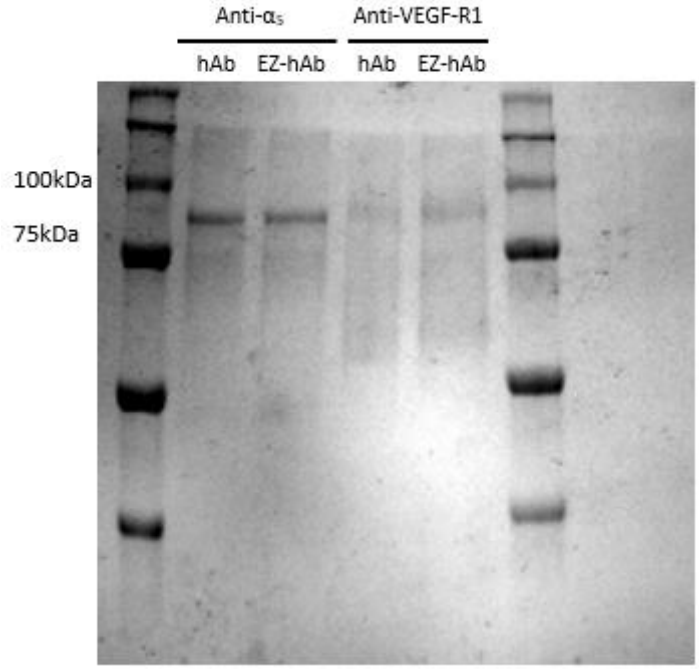

Figure 32: Antibody Reduction Result SDS-PAGE Gel. half antibody (hAb), EZ-link half antibody (EZ-hAb). Anti-α_5 is the SY09-09 antibody against the α_5 subunit of integrin $\alpha_5\beta_1$ and anti-VEGF-R1 is the SY-0909 antibody against the extracellular domain of VEGF-R1.

To verify the correct reduction of the antibodies used for the SPT experiment we need to run an 8% SDS-PAGE gel. A band at around 75-88kDa (as you can see in figure 32) indicates that the antibody has been reduced between the disulphide bonds that hold on together the two heavy chains meaning the resulting antibody will only have one light-chain and one heavy chain (See Figure 18). This will avoid artificial micro-clustering because the half antibody only has one variable region through which it can recognise the antigen.

We loaded the half antibody (hAb) and the antibody conjugated with the EZ-Link to see if we could observe any weight differences. In the four wells, you can see a smear starting at 150kDa, this is because not all the antibody has reduced exactly as we wanted because the reactions must be very exact and equimolar which is difficult to achieve. Nonetheless, the band with the most intensity lays between the right values. The VEGF-R1 band is less intense because the final concentration was 0.175ng/ml and the $\alpha_5\beta_1$ was of 0.281ng/ml.

9.2 Solid Barrier Biocompatibility

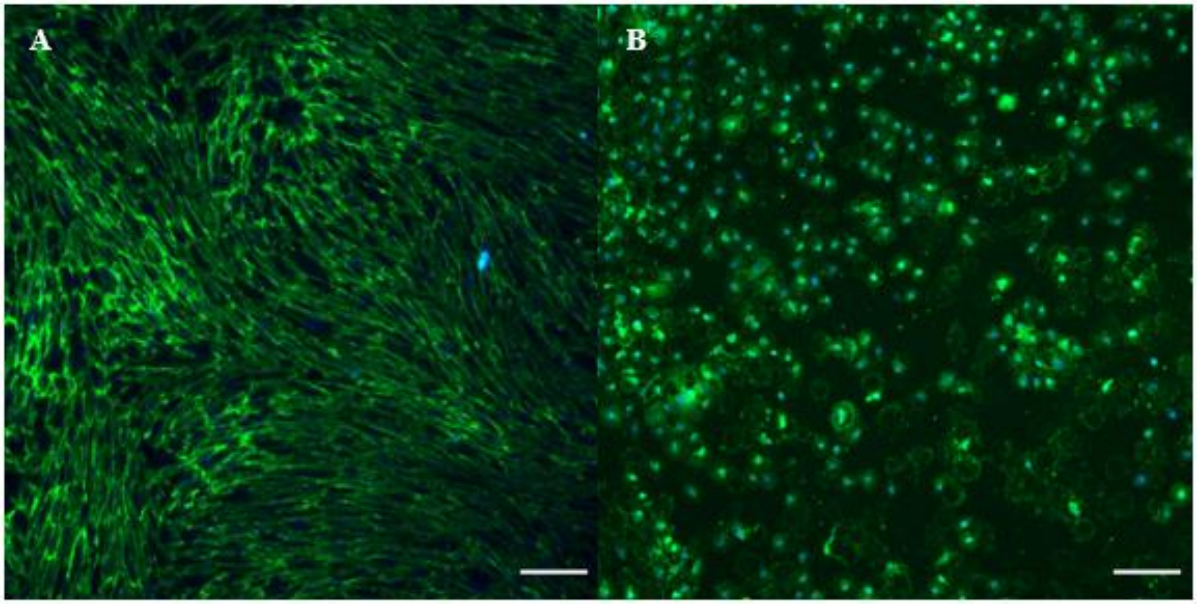

Figure 33: Solid Barrier Biocompatibility. (A) Human Dermo fibroblast on fibronectin/BSA coating after the removal of the solid barrier coated with PDMS. (B) Human Dermo fibroblast on fibronectin/BSA coating after the removal of the solid barrier without PDMS coating. Membrane stained with Concanavalin A-Alexa Fluor 488 (green) and nucleus with DAPI (blue). Epifluorescence images were taken at 10x and 20x respectively and the scale bar is 150μm in both images.

The resin manufacturer did not state clear if the resin was biocompatible or not so we decided to coat one of the solid barriers with PDMS (a biocompatible polymer) and carry out the wound healing assay as normal but with the difference that instead of recording the cells closing the gap, we stained them with DAPI (nucleus) and Concanavalin A-Alexa Fluor 488 (cell membrane and fibronectin coating). As we can see from figure 33 A, when the solid barrier was coated with PDMS fibroblast had a healthy and normal morphology. However, in figure 33 B, fibroblasts adopted a rounded morphology and cell density was reduced indicating clearly that the resin was cytotoxic for the cells. So, the wound healing assays were performed with a PDMS-coated solid barrier to avoid compromising the migration results.

9.3 Population Doubling Population

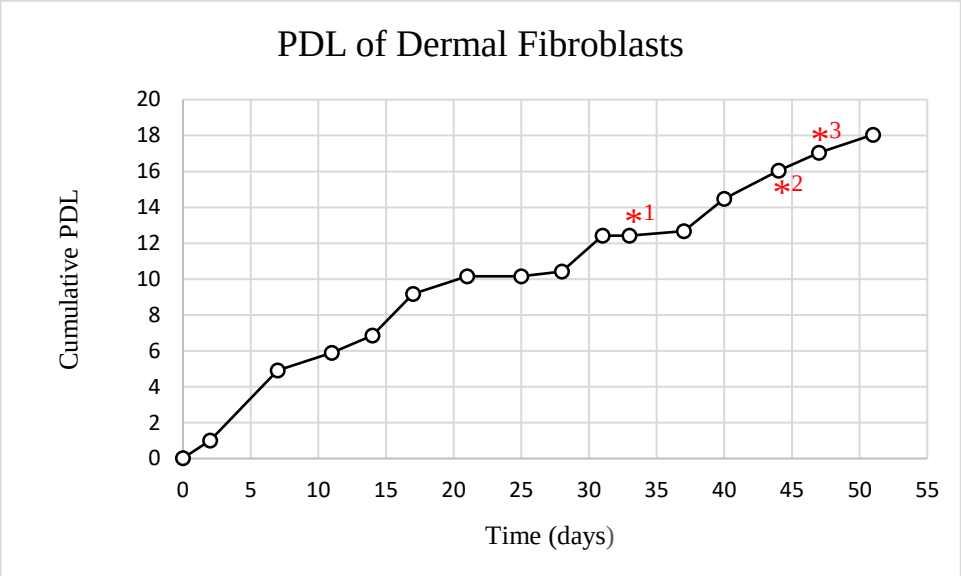

Figure 34: Population Doubling Level of Human Dermal Fibroblasts. Cumulative PDL was plotted against time (51 days.) *[1] indicates when the 15% wound healing assay was performed (PDL12); *[2] indicates when the wound healing assay with the VEGFA treatment was performed (PDL16); *[3] indicates when integrin $\alpha_1\beta_5$ diffusion experiment was performed (PDL17);

After every passage (trypsinization) cells were counted with a Neubauer chamber before re-seeding them in a new flask. PDL was calculated using the following formula:

$$PDL = 3{,}32 * \log\left(\frac{Final\ cell\ yield}{Seeded\ Cells}\right)$$

Where 'Final cells yield' are the number of cells after trypsinisation and 'Seeded cells' are the number of cells transferred to the new culture flask.

As you can see from figure 34, the cumulative PDL increases as time goes by but during the first days (0-20) this tendency is more pronounced, then the slope is less steep (20-51). If we had had the chance to continue calculating the PDL for longer we could see how eventually the line would be stabilized as in figure 9 A in section 1.4.4.1, this figure shows the PDL during 180 days.

9.4 Localization Precision

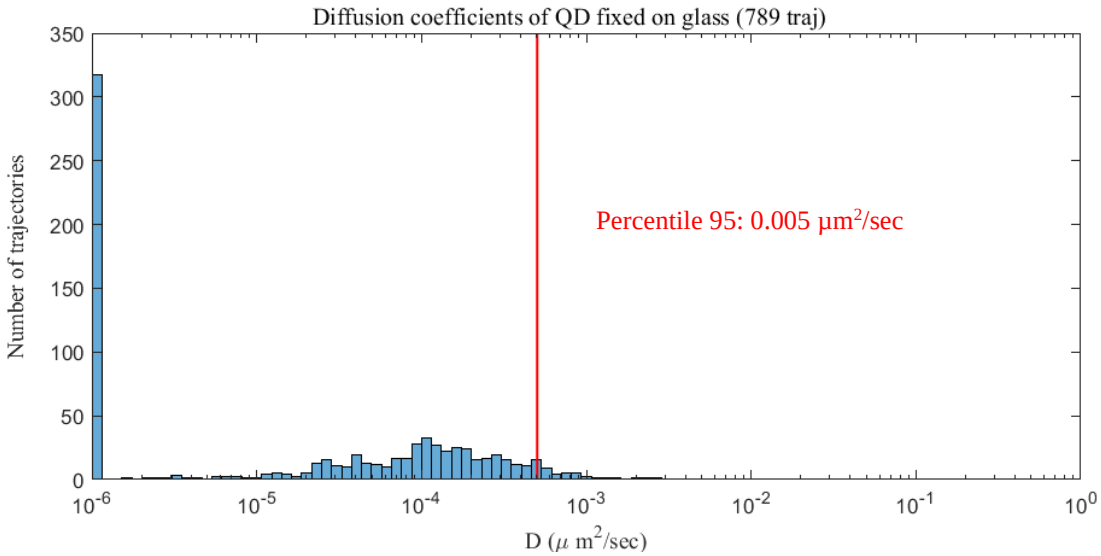

Figure 35: Diffusion Coefficient Histogram of QD on glass. The histogram shows the diffusion values of QD, the percentile 95 of these values was calculated and is shown with a red line on the histogram.

A histogram was plotted with the diffusion values of QD on glass and the percentile 95 of the diffusion values was calculated (0.0005µm^2/sec). This was used as the localization precision value. This parameter is used to distinguish between real movement and movement produced by external vibration of the room, the table where the microscope is placed on and other factors such as temperature.

9.5 Negative Moulds for Solid Barrier Wound Healing Assay

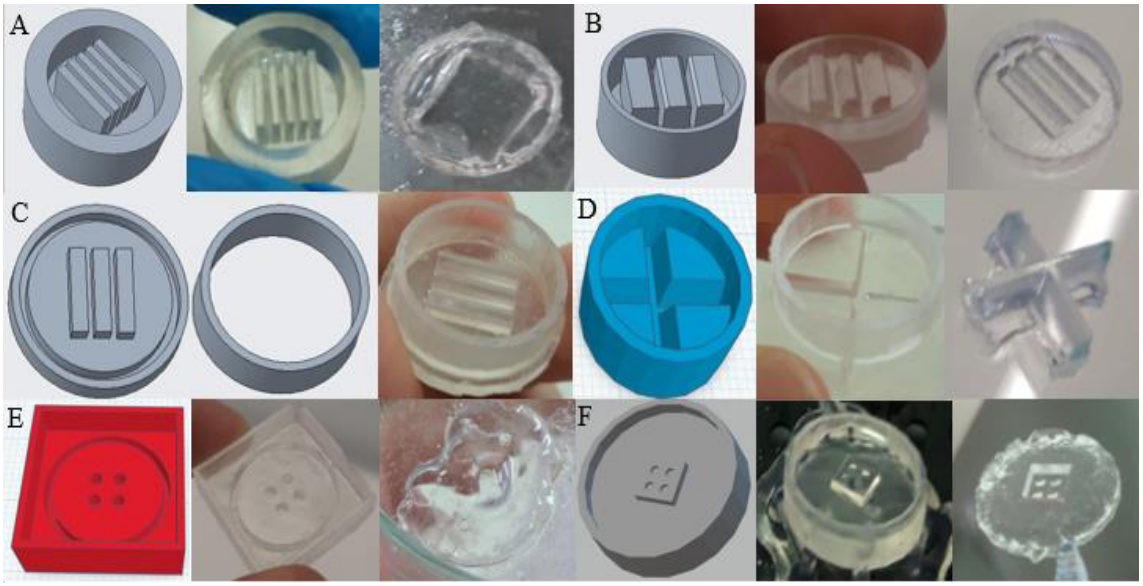

Figure 36: Negative moulds 3D printed for the wound healing assay solid barrier. This figure shows some of the negative moulds used to create solid barriers entirely out of PDMS, you can see the *PTC creo* design alongside the 3D printed mould and the PDMS outcome. (A) the PDMS barrier should have created rectangular wounds ;(B) an improved version of (A) ;(C) another version of (A) created to explore easy ways to unmould ;(D) the PDMS barrier created a cross-like shape ;(E) the PDMS barrier was supposed to create rounded wounds ;(F) An improved version of (E) that allowed the PDMS to cure.

At first, we created negative moulds and then poured PDMS to them and allow them to cure, the result was a solid barrier entirely made from PDMS. We started exploring this method of creating solid barriers based on what we read in the literature about this topic. We ran into some problems like the difficulty of unmoulding some of them like the one we can see on figure 36 A or that the mould did not allowed the PDMS to properly cure like the in the case of E. In total there were made eleven negative moulds based on the ones shown in Figure 36 but we slight variations between each other to try to solve the problems stated above.

The major problem we faced was that when we seeded the cells, was that the density of the PDMS was lower than the density of the culture medium so they floated but we could not make them bigger because they would have not fit inside the culture dish. The only solution we could think of to solve this problem was to add less culture medium. The medium that we could add before the PDMS barrier floated was so little that after 24h evaporated so cells' viability was compromised. So, in the end, we decided to 3D print directly the moulds (positive barriers) like the ones shown in Section 4.2.1 Figure 24.